

AD-A173 017

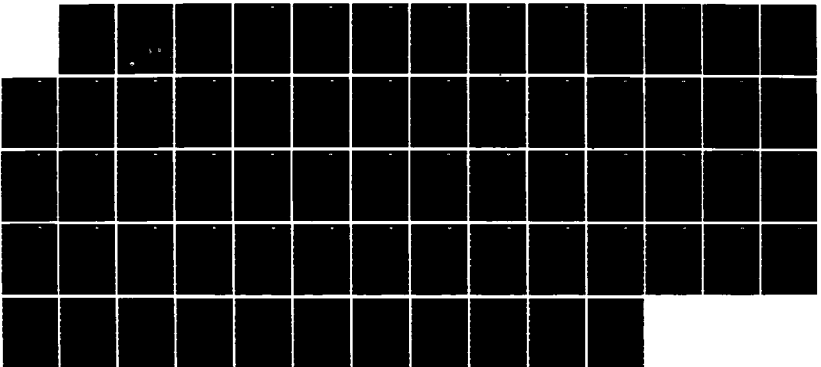
RESEARCH ON MILLIMETER WAVE DIELECTRIC MATERIALS(U)
ROCKWELL INTERNATIONAL THOUSAND OAKS CA SCIENCE CENTER
J R OLIVER ET AL. AUG 86 SC5345. AR N00014-81-C-0463

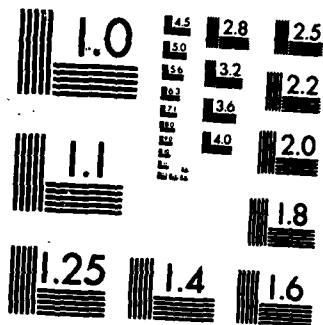
1/1

UNCLASSIFIED

F/G 20/2

NL





MICROCOPY RESOLUTION TEST CHART
NATIONAL BUREAU OF STANDARDS-1963-A

12

SC5345.AR

SC5345.AR

Copy No. 6

AD-A173 017

RESEARCH ON MILLIMETER WAVE DIELECTRIC MATERIALS

ANNUAL REPORT FOR THE PERIOD
March 1, 1985 through February 28, 1986

CONTRACT NO. N00014-81-C-0463

Prepared for

Material Sciences Division
Office of Naval Research
800 North Quincy Street
Arlington, VA 22217

J.R. Oliver
Principal Investigator

R.R. Neurgaonkar
Program Manager

DTIC
ELECTE
OCT 14 1986
S D

DISTRIBUTION STATEMENT A
Approved for public release
Distribution Unlimited

AUGUST 1986

Reproduction in whole or in part is permitted for any purpose of the
United States Government.



Rockwell International
Science Center

DTIC FILE COPY

86 9 30 05 7

UNCLASSIFIED

SECURITY CLASSIFICATION OF THIS PAGE

REPORT DOCUMENTATION PAGE

1a. REPORT SECURITY CLASSIFICATION Unclassified		1b. RESTRICTIVE MARKINGS AIM3017	
2a. SECURITY CLASSIFICATION AUTHORITY		3. DISTRIBUTION/AVAILABILITY OF REPORT Reproduction in whole or in part is permitted for any purpose of the United States Government.	
2b. DECLASSIFICATION/DOWNGRADING SCHEDULE			
4. PERFORMING ORGANIZATION REPORT NUMBER(S) SC5345.AR		5. MONITORING ORGANIZATION REPORT NUMBER(S)	
6a. NAME OF PERFORMING ORGANIZATION Rockwell International Science Center		6b. OFFICE SYMBOL (If applicable)	7a. NAME OF MONITORING ORGANIZATION
6c. ADDRESS (City, State and ZIP Code) 1049 Camino Dos Rios Thousand Oaks, CA 91360		7b. ADDRESS (City, State and ZIP Code)	
8a. NAME OF FUNDING/SPONSORING ORGANIZATION Material Sciences Division Office of Naval Research		8b. OFFICE SYMBOL (If applicable)	9. PROCUREMENT INSTRUMENT IDENTIFICATION NUMBER Contract No. N00014-81-C-0463
8c. ADDRESS (City, State and ZIP Code) 800 North Quincy Street Arlington, VA 22217		10. SOURCE OF FUNDING NOS.	
11. TITLE (Include Security Classification) RESEARCH ON MILLIMETER WAVE DIELECTRIC MATERIALS (U)		PROGRAM ELEMENT NO.	PROJECT NO. NR 032-609 (471)
12. PERSONAL AUTHOR(S) Oliver, J.R. and Neurgaonkar, R.R.		TASK NO.	WORK UNIT NO.
13a. TYPE OF REPORT Annual Report	13b. TIME COVERED FROM 03/01/85 TO 02/28/86	14. DATE OF REPORT (Yr., Mo., Day) AUGUST 1986	15. PAGE COUNT 73 ?
16. SUPPLEMENTARY NOTATION			
17. COSATI CODES		18. SUBJECT TERMS (Continue on reverse if necessary and identify by block number)	
FIELD	GROUP	SUB. GR.	
19. ABSTRACT (Continue on reverse if necessary and identify by block number)			
<p>Much of the early effort in this program was devoted to single crystal strontium barium niobate (SBN), a tungsten bronze with an unusually large room-temperature dielectric response. More recently, other tungsten bronzes such as potassium lithium niobate (KLN) and barium strontium potassium sodium niobate (BSKNN) have been prepared and studied to elucidate the role of unfilled crystallographic sites in influencing dielectric loss. Currently, we are developing preparation techniques for morphotropic phase boundary (MPB) bronzes, such as lead barium niobate (PBN), which should exhibit exceptionally large nonlinear electrical and optical response for a Pb:Ba ratio of 60:40, where it undergoes a transition from tetragonal to orthorhombic form.</p> <p>Large, high quality BSKNN single crystals have now been developed for free-space millimeter wave measurements. Measurements on BSKNN and SBN at room and cryogenic temperatures are reported, and a theoretical model has been successfully formulated for the dielectric response. Low frequency data are also presented for a new orthorhombic bronze, SCNN, which shows high suitability for millimeter wave development.</p>			
20. DISTRIBUTION/AVAILABILITY OF ABSTRACT UNCLASSIFIED/UNLIMITED <input checked="" type="checkbox"/> SAME AS RPT. <input type="checkbox"/> DTIC USERS <input type="checkbox"/>		21. ABSTRACT SECURITY CLASSIFICATION Unclassified	
22a. NAME OF RESPONSIBLE INDIVIDUAL		22b. TELEPHONE NUMBER (Include Area Code)	22c. OFFICE SYMBOL



TABLE OF CONTENTS

	<u>Page</u>
1.0 INTRODUCTION AND PROGRESS SUMMARY.....	1
2.0 MILLIMETER WAVE APPLICATIONS.....	4
3.0 MATERIALS DEVELOPMENT.....	6
3.1 Introduction.....	6
3.2 Importance of T.B. Family Materials.....	8
3.3 Growth of New Tungsten Bronze Compositions.....	9
3.3.1 Development of MPB Compositions for Millimeter Wave Studies.....	11
3.3.2 SCNN Single Crystals.....	17
3.3.3 BSKNN Single Crystals.....	20
4.0 MILLIMETER WAVE MEASUREMENTS AND THEORETICAL MODELING.....	24
4.1 Introduction.....	24
4.2 Millimeter Wave Dielectric Measurement Technique Development.....	24
4.3 Millimeter Wave Dielectric Properties of Single Crystal BSKNN.....	26
4.4 Progress Summary of Experimental Effort at UCLA.....	31
4.5 Theoretical Modeling.....	36
4.5.1 Dielectric Permittivity and Loss.....	36
4.5.2 Electric Field Sensitivity.....	40
5.0 CONCLUSIONS AND RECOMMENDATIONS.....	43
6.0 FUTURE PLANNED RESEARCH.....	44
7.0 PUBLICATIONS AND PRESENTATIONS.....	46
7.1 Publications.....	46
7.2 Presentations.....	47
8.0 REFERENCES.....	48
APPENDICES	
1 Structural and Ferroelectric Properties of Morphotropic Phase Boundary Systems in the Tungsten Bronze Family.....	1-1
2 Millimeter Wave Dielectric Properties of Tungsten Bronze Ferroelectrics at 77K and 300K.....	2-1
3 Electro-Optic Devices for Millimeter Wave Using Cooled Ferroelectrics.....	3-1
4 Millimeter Wave Absorption and Refraction in Tungsten Bronze Ferroelectrics.....	4-1

etc. on file

/ Codes

and/or
Special

Di. t

A-1





LIST OF FIGURES

<u>Figure</u>		<u>Page</u>
1	Room temperature dielectric constant for ceramic compositions in the $Ba_2NaNb_5O_{15}$ - $Sr_2NaNb_5O_{15}$ - $Ca_2NaNb_5O_{15}$ solid solution system.....	10
2	Curie phase transition temperature for tungsten bronze $Pb_{1-x}Ba_xNb_2O_6$	13
3	Piezoelectric properties for tungsten bronze $Pb_{1-x}Ba_xNb_2O_6$	13
4	Dielectric constant at 10 kHz for hot-pressed ceramic PBLN (60/40/6) poled at 20 KV/cm. Upper curve is for the direction perpendicular to the pressing axis (dashed - depoled); lower curve is parallel to the pressing axis.....	15
5	X-ray diffraction spectrum of hot-pressed PBLN (60/40/6) for face normals parallel and perpendicular to the pressing axis. Note the absence of (hkl) and (hk2) lines in the upper figure.....	16
6	Dielectric constant for single crystal SCNN (190/10). Solid curve is for $\langle 001 \rangle$ axis at 10 kHz (largely independent of frequency). Dashed curves are for the $\langle 110 \rangle$ axis at 0.1, 1.0, 10 and 100 kHz.....	18
7	Polarization and pyroelectric behavior of c-axis SCNN (190/10) as a function of temperature.....	19
8	Dielectric constant at 10 kHz for a- and c-axis BSKNN-2 single crystals poled at 10 kV/cm. Dashed curve is for thermally depoled c-axis crystal.....	21
9	Spontaneous polarization for c-axis BSKNN-2 as a function of temperature.....	22
10	Schematic of the free-space millimeter wave dielectric characterization apparatus.....	25
11	33-50 GHz transmission of c-axis BSKNN-2 at room temperature. $t = 0.0445$ cm.....	28



LIST OF FIGURES

<u>Figure</u>		<u>Page</u>
12	33-50 GHz reflection of c-axis BSKNN-2 at room temperature.....	28
13	33-50 GHz reflection of c-axis BSKNN-2 at 77K.....	29
14	33-50 GHz reflection of a-axis BSKNN-2 at room temperature.....	29
15	55-110 GHz refractive index n as a function of temperature for SBN:60 (circles), BSKNN-1 (triangles) and BSKNN-2 (squares). Open symbols are for the a-axis, closed for the c-axis.....	32
16	55-110 GHz absorption index k as a function of temperature for SBN:60 (circles), BSKNN-1 (triangles) and BSKNN-2 (squares). Open symbols are for the a-axis, closed for the c-axis.....	33
17	Transmittance as a function of frequency and applied DC voltage for BSKNN at room temperature.....	34
18	Transmittance change as a function of frequency for BSKNN at 3.5 kV at room temperature.....	35
19	Comparison of transmittance change for SBN:60 at 3.5 kV at 35 and 297K.....	35



LIST OF TABLES

<u>Table</u>		<u>Page</u>
1	Dielectric Properties of Tungsten Bronze Crystals.....	7
2	Ferroelectric Properties at MPB for Various Tungsten Bronze Systems.....	8
3	Millimeter Wave Dielectric Properties of Single Crystal BSKNN-2.....	30
4	Millimeter Wave Dielectric Properties of Single Crystal BSKNN and SBN.....	37
5	Trends in Polar Axis Loss Ratio $\epsilon_0 \epsilon'' / (\epsilon')^2$ at 30-50 GHz Compared with Acoustic Loss Model.....	40
6	Electric Field Sensitivity of the Polar Axis Refractive Index at 100 GHz.....	41



1.0 INTRODUCTION AND PROGRESS SUMMARY

High permittivity ferroelectric materials such as the tungsten bronzes and perovskites have shown substantial promise for the manipulation and control of electromagnetic propagation properties at frequencies from dc to the infra-red. In the last few years, interest has grown in millimeter wave applications for communications and radars, and a need has developed to characterize the linear and nonlinear dielectric properties of ferroelectrics in this new frequency range.

The research effort herein is part of a long-range program whose objective is to determine the range of dielectric properties attainable at millimeter wave frequencies in various classes of high permittivity ferroelectrics, and to relate these properties to fundamental crystal characteristics. This work involves the preparation of new ferroelectrics in single crystal and ceramic form, characterization of their crystal structure and low frequency dielectric response, and measurement of both linear and nonlinear dielectric properties at millimeter wave frequencies.

Much of the early effort in this program was devoted to single crystal strontium barium niobate (SBN), a tungsten bronze with an unusually large room-temperature dielectric response. More recently, other tungsten bronzes such as potassium lithium niobate (KLN) and barium strontium potassium sodium niobate (BSKNN) have been prepared and studied to elucidate the role of unfilled crystallographic sites in influencing dielectric loss. Currently, we are developing preparation techniques for morphotropic phase boundary (MPB) bronzes, such as lead barium niobate (PBN), which should exhibit exceptionally large nonlinear electrical and optical response for a Pb:Ba ratio of 60:40, where it undergoes a transition from tetragonal to orthorhombic form.

During the past year, significant progress was made in materials development, millimeter wave dielectric characterization and theoretical modeling efforts. These include:



SC5345.AR

1. Successful growth of large-size high optical quality single crystal BSKNN suitable for free space millimeter wave measurements.
2. Development of free space experimental methods for accurate determination of the millimeter wave response of ferroelectric materials at room and cryogenic temperatures.
3. First complete experimental determination of the millimeter wave dielectric and dn/dE values for BSKNN at room and cryogenic temperatures for various crystal orientations.
4. Successful hot-pressing of very large size high quality, grain oriented semi-transparent ceramics of PBN:60 (2.5×2.5 cm).
5. Successful formulation of a theoretical model for millimeter wave dielectric response in single crystal tungsten bronzes.

These results are extremely encouraging for basic understanding of the mechanism controlling millimeter wave susceptibilities in ferroelectric tungsten bronzes as well as for practical applications. We have shown, as was the case for SBN in our previous work, that single crystal BSKNN is potentially suitable for millimeter wave devices, particularly at low temperatures. In addition, the experimental data base generated for this material has allowed the construction and verification of a modeling framework for the dielectric response and its electric field dependence as a function of temperature.

In addition to exploring the millimeter wave dielectric properties of morphotropic phase boundary materials, our work in the coming year will include three major efforts. First, measurements of the temperature dependence of dn/dE will be extended to BSKNN and other available ferroelectrics through the technique of free-space measurements on mosaic samples. Second, evaluation of the potential of these materials for beam steering, modulation, and other functions



Rockwell International
Science Center

SC5345.AR

will be carried out at UCLA. Third, calculations based on the coupling of spatially varying spontaneous polarization to acoustic phonons will be carried out to evaluate the effect of such variations on the dielectric properties of ferroelectrics.



SC5345.AR

2.0 MILLIMETER WAVE APPLICATIONS

The large nonlinear susceptibility observed in various ferroelectric single crystals developed in this program makes them ideally suited for millimeter wave active device applications. The phase shifts which can be produced by an externally applied electric field on these materials can be utilized for beam-steering in dielectric lenses and phased-array antennas, while the inherent nonlinear dielectric response can be used for frequency doubling and frequency mixing purposes. Potential advantages in these applications include very fast response times and the ability to handle high power levels without damage or saturation.

Advances in materials research and dielectric characterization during last year's effort in this program have resulted in substantial improvements in the properties of single crystal SBN and BSKNN such that practical devices are now potentially feasible. Consequently, it is now worthwhile to carry out exploratory device development in order to demonstrate the utility of these classes of materials for millimeter wave applications. Towards this objective, a minimum effort will be undertaken to design, fabricate and test a microwave strip-line circuit for beam steering. This effort will be performed at UCLA by Professor Harold Fetterman of the E.E. Department and will be aimed primarily at proof-of-principle laboratory demonstration of the device concept, rather than optimization of performance parameters.

The successful growth of large, high optical quality single crystal ferroelectrics with improved millimeter wave and optical properties also makes possible the superposition of millimeter wave phase and amplitude modulation onto an optical carrier beam. In particular, the visible wavelength electro-optic coefficients of SBN:75 have been determined to be sufficiently large, such that the electric field strengths associated with moderate-power microwave beams (1 - 10 W) are sufficient to cause a significant change in the optical index of the material. This change, in turn, can be used to modulate the phase of an optical beam, resulting in frequency and/or amplitude modulation of the optical



SC5345.AR

signal. To further explore this concept, a Rockwell funded IR&D program is currently planned for FY 1987. This experimental effort will consist of focusing a millimeter wave beam onto a single crystal sample and passing a visible wavelength laser beam nearly orthogonal to the incoming millimeter wave direction. The relative angles of the beams will be adjusted to match the optical and modulation field phase velocities. The transmitted laser beam will then be frequency-analyzed with a Fabry-Perot resonator to determine the amplitudes of the millimeter wave side-bands. Studies will be carried out to determine conversion efficiency as functions of millimeter wave frequencies and material parameters. Ferroelectric single crystals showing the most promise will be examined, including SBN and BSKNN. Potential device and system applications resulting from this concept include: super high frequency modulation of optical signals; millimeter wave transmission by fiber-optic techniques; and processing of millimeter wave signals using optical techniques.



3.0 MATERIALS DEVELOPMENT

3.1 Introduction

A goal of this research program is to develop classes of ferroelectric materials which are suitable to develop a better understanding of high frequency dielectric properties and also useful for future device studies. The following criteria have been chosen to select compositions for high frequency dielectric studies:

1. Large dn/dE at high frequencies
2. Large electro-optic coefficient
3. Large dielectric constant at low and high frequencies
4. Low dielectric losses at low and high frequencies.

In addition to SBN:60 and BSKNN, new perovskite and tungsten bronze crystals, along with grain oriented dense ceramics which are close to morphotropic phase boundary (MPB) regions, are under development. These include:

1. Large Electro-Optic Coefficient Materials

$Sr_{0.75}Ba_{0.25}Nb_2O_6$ (SBN:75)	Tetragonal Bronze
$Pb_{0.6}Ba_{0.4}Nb_2O_6$ (PBN:60)	Tetragonal Bronze
$Pb_{0.7}Ba_{0.3}Nb_2O_6$ (PBN:60)	Orthorhombic Bronze
$KNbO_3$	Orthorhombic Perovskite
$KTa_{1-x}Nb_xO_3$ (KTN)	Tetragonal Perovskite
$Sr_{2-x}Ca_xNaNb_5O_{15}$	Orthorhombic Bronze



2. Morphotropic Phase Boundary Systems (Bronze)

- $PbNb_2O_6$ - $Sr_2NaNb_5O_{15}$ (Orthorhombic-Orthorhombic)
 $Sr_2NaNb_5O_{15}$ - $Ba_2NaNb_5O_{15}$ (Orthorhombic-Orthorhombic)
 $Sr_2NaNb_5O_{15}$ - $Pb_2KNb_5O_{15}$ (Orthorhombic-Orthorhombic)

Based on our present research in the tungsten bronze and perovskite families, most of these compositions exhibit low dielectric losses with high dielectric and electro-optic coefficients at low frequencies. The systematic growth and characterization of these ferroelectric materials is an ongoing and important part of several current programs, including the present. Tables 1 and 2 give a brief summary of the tungsten bronze family compositions selected for the present work.

Table 1
Dielectric Properties of Tungsten Bronze Crystals

Crystal	T_c (°C)	Dielectric Constant ϵ_{33}	Electro-Optic Coefficient $\times 10^{-12}$ m/V	dn/dE		Crystal Size
				295K	77K	
$Sr_{0.75}Ba_{0.25}Nb_2O_6$ (SBN:75)	56	3400	1400	Large*		1-2 cm
$Sr_{0.6}Ba_{0.4}Nb_2O_6$ (SBN:60)	78	900	420	2×10^{-6}	5×10^{-7}	2-3 cm
BSKNN-2	209	180	$r_c > 2000$	4×10^{-7}	4×10^{-8}	1-1.2 cm
$Sr_2KNb_5O_{15}$ (SKN)	150	1000	180	-	-	0.5-0.8 cm
$K_3Li_2Nb_5O_{15}$ (KLN)	405	120	70	-	-	0.5-0.8 cm
$Sr_{2-x}Ca_xNaNb_5O_{15}$ *	270	> 1700	> 2000	Large*		0.4-0.6 cm

*Expected large values of dn/dE



Table 2
Ferroelectric Properties at MPB for Various Tungsten Bronze Systems

System	X at MPB	T _c (°C)	Dielectric Constant at R.T.	Electro-Optic Coefficient x 10 ⁻¹² m/V	Application
(1-x) PbNb ₂ O ₆ - (x)BaNb ₂ O ₆	La ³⁺ (2%)	300	-	-	
		230	1700	420	MW + EO
		115	3500	780	MW + EO
(1-x) PbNb ₂ O ₆ - (x)Sr ₂ NaNb ₅ O ₁₅	0.75	130	2200	Large	MW + EU
(1-x) Pb ₂ KNb ₅ O ₁₅ - (x)Ba ₂ NaNb ₅ O ₁₅	0.25	255	1340	Large	MW + EO
(1-x) Pb ₂ KNb ₅ O ₁₅ - (x)Sr ₂ NaNb ₅ O ₁₅	0.70	148	930	Medium	MW + Pyro

MW = Millimeter Wave
EO = Electro-Optic
Pyro = Pyroelectric

3.2 Importance of T.B. Family Materials

The tungsten bronze family embraces some 150 known compounds and several solid-solution systems, and thus offers a wide variety of materials. Some of the unique advantages of bronze crystals for millimeter wave studies are as follows:

1. This family of crystals possess extraordinarily large transverse and longitudinal electro-optic and dielectric properties, specifically near an MPB region.
2. Trade-off between dn/dE , dielectric constant and $\tan\delta$ can be investigated for millimeter wave studies due to structural flexibility. Furthermore, in the T.B. structure, several crystallographic sites, specifically the 15- and 12-fold coordinated sites, are partially empty, which allows the composition to be tailored.



3. Several ferroelectric MPB systems have been identified and established for this family.
4. The lower prototype symmetry gives a large family of dielectric constants and the possibility of anisotropic conduction. The nonzero values are ϵ_{11} , ϵ_{12} , ϵ_{13} , ϵ_{44} and ϵ_{66} , as compared to ϵ_{11} , ϵ_{12} and ϵ_{44} in perovskites.
5. In the tetragonal bronzes, since the prototype symmetry is $4mm$, only one unique 4-fold axis exists and 90° twins are absent; hence crystals are not likely to crack during poling as reported for $BaTiO_3$.

3.3 Growth of New Tungsten Bronze Compositions

To date, our work has heavily concentrated on three different ferroelectric bronze compositions, specifically SBN:60 (partially unfilled 15- and 12-fold sites), BSKNN (15- and 12-fold sites completely filled) and KLN (all sites completely filled). High frequency measurements have been performed from liquid nitrogen to the Curie temperature, and the information obtained has contributed to our understanding of these materials and has indicated potential device applications. Further work is being carried out in these materials to establish their dn/dE behavior at low temperatures.

In addition to these crystals, we are developing three other important tungsten bronze materials, specifically, $Sr_{0.75}Ba_{0.25}Nb_2O_6$ (SBN:75), $Pb_{0.6}Ba_{0.4}Nb_2O_6$ (PBN:60) and $Sr_{2-x}Ca_xNaNb_5O_{15}$ (SCNN) for millimeter wave studies. Since the dielectric constants for these crystals are significantly higher than for many previously studied bronzes, it is expected that both a large dielectric constant and a higher dn/dE can be maintained at millimeter wave frequencies.

SCNN single crystals are being introduced for the first time in this study. We expect that this system is likely to become important for millimeter wave and optical applications, since the addition of Ca^{2+} in the orthorhombic



SC5345.AR

$\text{Sr}_2\text{NaNb}_5\text{O}_{15}$ phase appears to significantly enhance the dielectric and electro-optic properties. Figure 1 shows the compositional dependence of the dielectric constant for the $\text{Ba}_2\text{NaNb}_5\text{O}_{15}$ - $\text{Sr}_2\text{NaNb}_5\text{O}_{15}$ - $\text{Ca}_2\text{NaNb}_5\text{O}_{15}$ system.

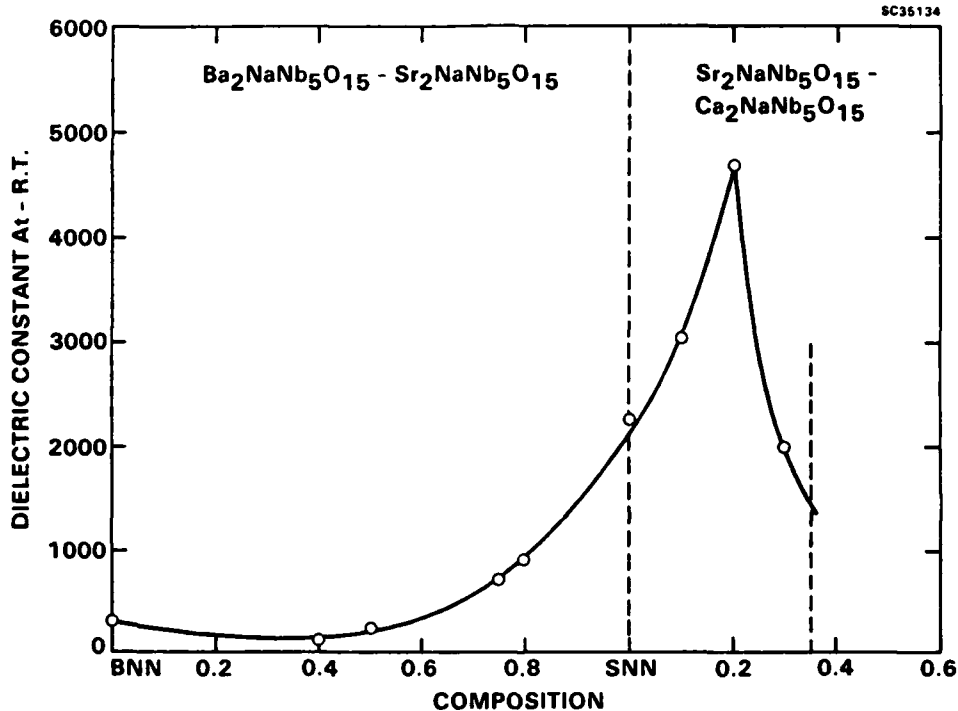


Fig. 1 Room temperature dielectric constant for ceramic compositions in the $\text{Ba}_2\text{NaNb}_5\text{O}_{15}$ - $\text{Sr}_2\text{NaNb}_5\text{O}_{15}$ - $\text{Ca}_2\text{NaNb}_5\text{O}_{15}$ solid solution system.

Current bulk single crystal work undertaken in DARPA and IR&D programs indicates that the substitution of Ca^{2+} in the $\text{Sr}_2\text{NaNb}_5\text{O}_{15}$ system allows flexibility in the control of both longitudinal and transverse properties. This flexibility could be of particular value in future millimeter wave applications.

The growth of PBN:60, SBN:75 (tetragonal) and SCNN (orthorhombic) crystals is a part of our on-going research under ONR, DARPA and IR&D Programs, and these crystals will be available as needed. Although both SBN:75 and SCNN possess attractive properties, as summarized in Table 1, they are not



SC5345.AR

considered to be congruent melting compositions; nevertheless, crystal growth of these compositions has been successful. As a matter of fact, our current ADC-equipped Czochralski apparatus is now capable of pulling optical quality doped and undoped SBN:75 crystals. These crystals have been shown to be very useful for photorefractive applications and several new device concepts have been proposed. Since SCNN is orthorhombic at room temperature, its growth is comparatively more difficult than for SBN:75. However, we have managed to grow around 0.5 to 0.7 cm diameter SCNN crystals of reasonable quality. This crystal has a large c-axis dielectric constant at room temperature (> 1700), and based on current calculations, we believe this crystal will have an electro-optic coefficient of over 2000 at room temperature.

In the case of BSKNN crystals, low frequency measurements show that the ϵ_{11} increases while ϵ_{33} decreases as one cools below room temperature. We expect that cooling this sample further below 77K, there is a possibility of establishing another phase transition which may be tetragonal to orthorhombic, since the end member composition $\text{Sr}_2\text{NaNb}_5\text{O}_{15}$ is orthorhombic at room temperature.

The current status of PBN, SCNN and BSKNN-2 materials development are summarized in the following sections.

3.3.1 Development of MPB Compositions for Millimeter Wave Studies

An approach to the development of improved millimeter wave materials is the use of morphotropic phase boundary (MPB) crystal compositions which have very large electro-optic effects. The electro-optic and dielectric properties close to the MPB regions are potentially 5 to 10 times better than the current best materials studied for millimeter wave applications, such as BSKNN, SBN:60 or BaTiO_3 , and offer a unique opportunity to develop superior millimeter wave materials. Figure 2 shows the phase diagram for ferroelectric tungsten bronze $\text{Pb}_{1-x}\text{Ba}_x\text{Nb}_2\text{O}_6$, in which the MPB region is located at $x = 0.37$. In this region, the electro-optic, dielectric, pyroelectric and piezoelectric properties are exceptionally large and are largely temperature independent.



SC5345.AR

As shown in Fig. 2, on a binary phase diagram an MPB appears as a nearly vertical line separating two ferroelectric phases, i.e., the boundary occurs at a nearly constant composition over a wide temperature range up to the Curie temperature. Poled crystals near such boundaries show unique and enhanced electro-optic properties because of the proximity in free energy of an alternative ferroelectric structure. Some of the unique advantages of MPB systems are as follows:

- Electro-optic, dielectric, piezoelectric and other properties are exceptionally large near the MPB region; hence, potentially large dn/dE and dielectric constants at millimeter wave frequencies can be found.
- For tetragonal compositions close to the boundary, longitudinal r_{51} and r_{42} values are larger than those for $BaTiO_3$ crystals.
- T.B. morphotropic systems, except Pb^{2+} -containing, are relatively easier to grow and fabricate in single crystal form as compared to perovskites.

Theoretical and experimental work has shown an enhancement of the ferroelectric properties of PBN near the MPB between the ferroelectric orthorhombic ($mm2$) and tetragonal ($4mm$) structure near the composition $Pb_{0.6}Ba_{0.4}Nb_2O_6$. As shown in Fig. 3, both the piezoelectric strain coefficients d_{15} and d_{33} increase as one approaches the boundary, indicating that the corresponding electro-optic coefficients r_{51} and r_{33} will also be large. The MPB composition $Pb_{0.6}Ba_{0.4}Nb_2O_6$ (PBN:60) has been prepared using both ceramic hot-pressing and Czochralski techniques; however, in the case of the Czochralski technique, the loss of Pb^{2+} is still a significant problem which severely affects homogeneity. For this reason, our work on PBN has emphasized the use of the hot-pressing technique.

Hot-pressed ceramic densification has been effectively used for ferroelectric material development since materials can be easily fabricated in a variety of sizes and shapes with good compositional control. In the case of

SC5345,AR

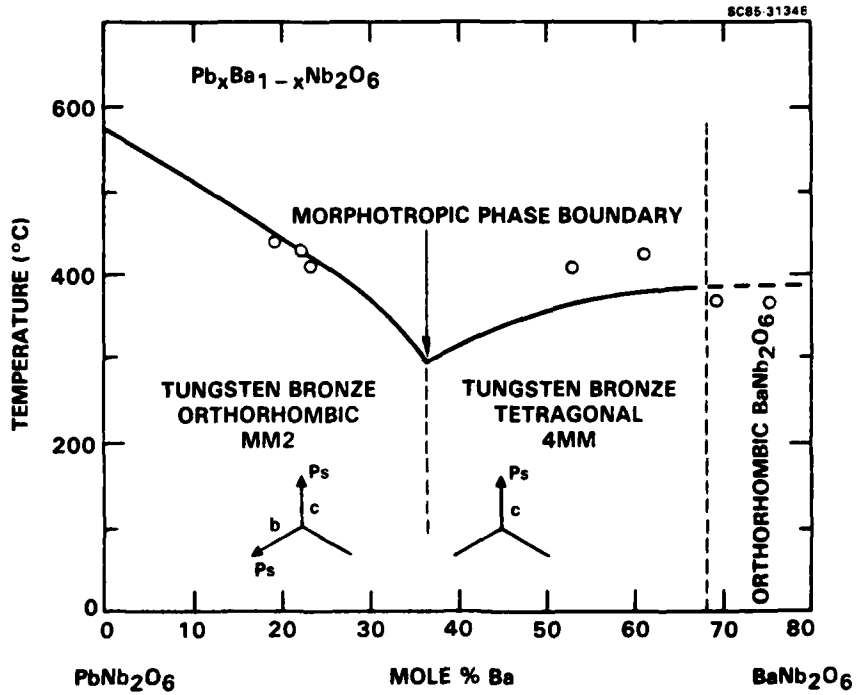


Fig. 2 Curie phase transition temperature for tungsten bronze $Pb_{1-x}Ba_xNb_2O_6$.

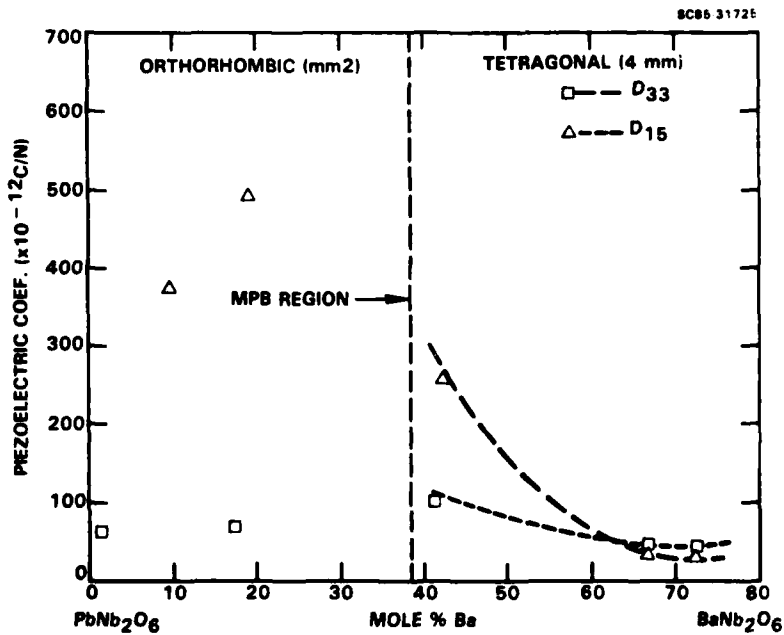


Fig. 3 Piezoelectric properties for tungsten bronze $Pb_{1-x}Ba_xNb_2O_6$.



PBN:60, our work on the hot-pressed densification of this bronze in the current program has been significantly enhanced by the use of an oxygen atmosphere uniaxial hot press. In contrast to previous growths with an inductively heated, graphite-die press, the present unit permits the ceramic densification of materials without the use of extensive post-growth oxidation. However, the use of alumina dies in the present unit necessitated a considerable amount of work on die design, material buffering (with alumina or zirconia powders), and in-situ annealing procedures in order to avoid ceramic and/or die cracking; this work was performed earlier under our IR&D program.

Recent ceramic densifications of La^{3+} -modified PBN:60 under the present program have been highly successful. An example of the dielectric properties for axial directions perpendicular and parallel to the pressing direction are shown in Fig. 4 for PBN:60 with 6% La^{3+} modification. The use of La^{3+} -modified material comes from two considerations: first, lanthanum modifications are now known to significantly improve the optical transparency and grain boundary interface properties of ceramic materials such as PZT and PBN; and second, lanthanum modification of PBN can significantly reduce the ferroelectric phase transitions temperature, T_c , resulting in a considerable increase of the polar axis dielectric constant at room temperature. In the case of PBLN(60/40/6) shown in Fig. 4, T_c has been reduced to 115°C from the unmodified PBN:60 value of approximately 280°C . As a result, the room temperature dielectric constant for the perpendicular direction is 4400 (poled) at room temperature, a factor of considerable significance for future millimeter wave applications.

The solid curves in Fig. 4 are dielectric data for poled ceramic samples. Poling was accomplished in dry oxygen with an electric field of 20 kV/cm applied during slow cooldown from 140°C to room temperature. Breakdown and/or excessive poling currents were not problems. The dashed curve in Fig. 4 also indicates the measured dielectric constant for the perpendicular direction in a thermally depoled condition. The difference in dielectric properties between poled and depoled conditions is typical of most tungsten bronzes; however, a frequency-dependent relaxor behavior, also typically found in bronzes such as SBN:60, is not strongly evident for PBLN (60/40/6), even in

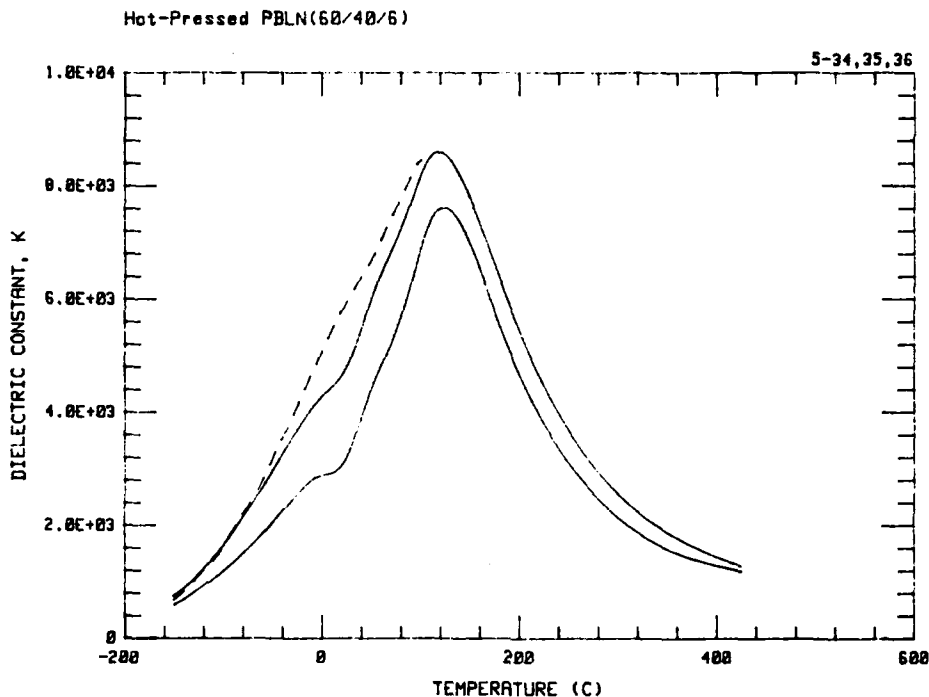


Fig. 4 Dielectric constant at 10 KHz for hot-pressed ceramic PBLN (60/40/6) poled at 20 kV/cm. Uper curve is for the direction perpendicular to the pressing axis (dashed-depoled); lower curve is parallel to the pressing axis.

a thermally depoled condition. Dielectric losses at room temperature are low, in the range of 0.01-0.03, for both axial directions.

An interesting fact in the dielectric data for PBLN (60/40/6) is that only moderate dielectric anisotropy observed, unlike the more strongly anisotropic PBLN compositions which have less La^{3+} modification. Initially, it was felt that this reflected only moderate grain orientation in hot-pressed PBLN (60/40/6). However, careful evaluation of x-ray diffraction measurements on samples with face normals perpendicular and parallel to the pressing axis, shown in Fig. 5, indicate nearly complete grain orientation. In Fig. 5, the parallel

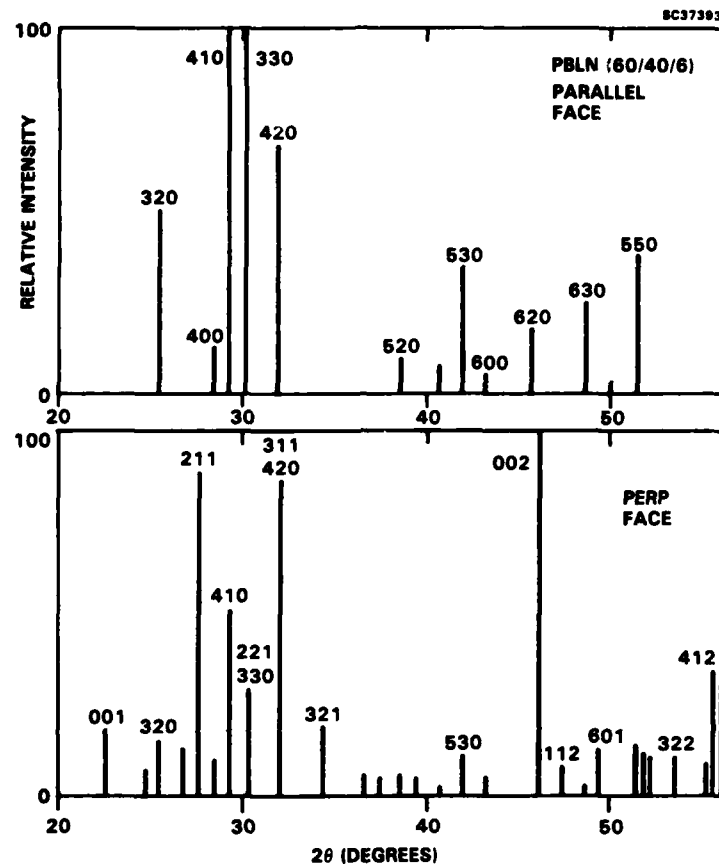


Fig. 5 X-ray diffraction spectrum of hot-pressed PBLN (60/40/6) for face normals parallel and perpendicular to the pressing axis. Note the absence of (hk1) and (hk2) lines in the upper figure.

cut sample shows a complete absence of (hk1) and (hk2) lines, whereas the perpendicular cut shows all (hk1) lines, indicating that the c -axis of the ceramic grains is oriented in the plane perpendicular to the pressing direction. An excellent fit to these data is obtained for tetragonal lattice constants of a , b = 12.543Å and c = 3.924Å; these are to be compared with the lattice constants for unmodified ceramic PBN:60 of a , b = 12.535Å and c = 3.978Å.

These results return us to the original question of the relatively low dielectric anisotropy observed for hot-pressed PBLN (60/40/6). It appears that the presence of 6% La^{3+} , coupled with reduced Pb^{2+} losses and oxygen atmosphere pressing, has resulted in material which is very nearly morphotropic; indeed,



poling of samples cut perpendicular and parallel to the pressing direction resulted in significant changes in the room temperature dielectric constants and dielectric loss for both directions.

These are very encouraging results, and represent a considerable improvement over previous hot-pressed ceramic densifications of PBN and PBLN. However, the present growths still contain significant numbers of pores which appear visually as a cloudiness to the otherwise nearly transparent, pale yellow color of polished samples. Such ceramic defects contribute greatly to high millimeter wave losses, and must be eliminated before further millimeter wave characterization can proceed. Presently, we are exploring changes in the hot pressing parameters, particularly temperature (1280-1300°C), excess PBO content (2-5%), and pressing time (3-6 h) to obtain better material.

3.3.2 SCNN Single Crystals

The tungsten bronze solid solution $\text{Sr}_{2-x}\text{Ca}_x\text{NaNb}_5\text{O}_{15}$ (SCNN) is based on the enhancement of the dielectric properties for orthorhombic $\text{Sr}_2\text{NaNb}_5\text{O}_{15}$ with Ca^{2+} substitution, as shown earlier in Fig. 1. Dielectric and polarization measurements have now been carried out on several small SCNN crystals which were grown by the Czochralski technique; Fig. 6 shows the low frequency dielectric constant vs temperature for two different orientations of $\text{Sr}_{1.9}\text{Ca}_{0.1}\text{NaNb}_5\text{O}_{15}$ (SCNN(190/10)). Along the $\langle 001 \rangle$, or \underline{c} axis, SCNN shows two prominent dielectric peaks, the largest being the strong first-order paraelectric/ferroelectric transition at 270°C shown in Fig. 6. The temperature of this phase transition is remarkably unaffected by Ca substitution for Sr up to the solubility limit. A second peak occurs between 50 - 100°C, depending on Ca content, and this is now believed to be a ferroelastic transition. Below room temperature, the dielectric constant declines to a large, nearly temperature-independent value of approximately 500.

The low frequency dielectric constant along the \underline{c} axis is essentially independent of frequency over the range covered (100 Hz - 100 kHz) at any given temperature. Such is not the case for other axial orientations such as the $\langle 110 \rangle$ direction, also shown in Fig. 6. In this direction, the two prominent

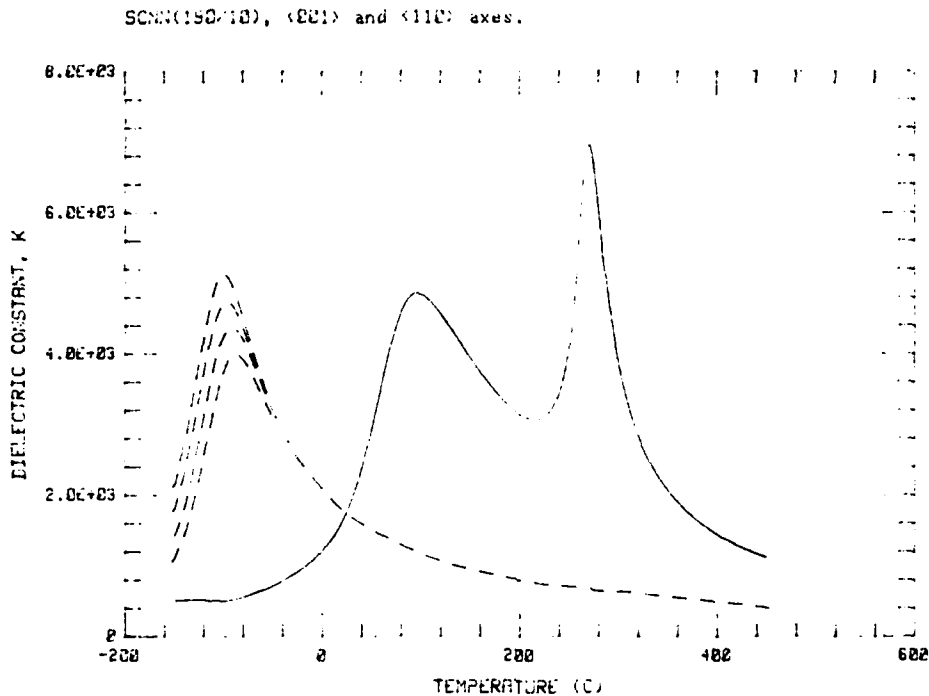


Fig. 6 Dielectric constant for single crystal SCNN (190/10). Solid curve is for <001> axis at 10 kHz (largely independent of frequency). Dashed curves are for the <110> axis at 0.1, 1.0, 10 and 100 kHz.

peaks observed along the c axis are not observed. Instead, the dielectric constant rises nearly monotonically with decreasing temperature, and achieves a large, frequency-dependent maximum in the range of -88 to -100°C. Such behavior indicates a probable freeze-out of the polarizability rather than the presence of another phase transition.

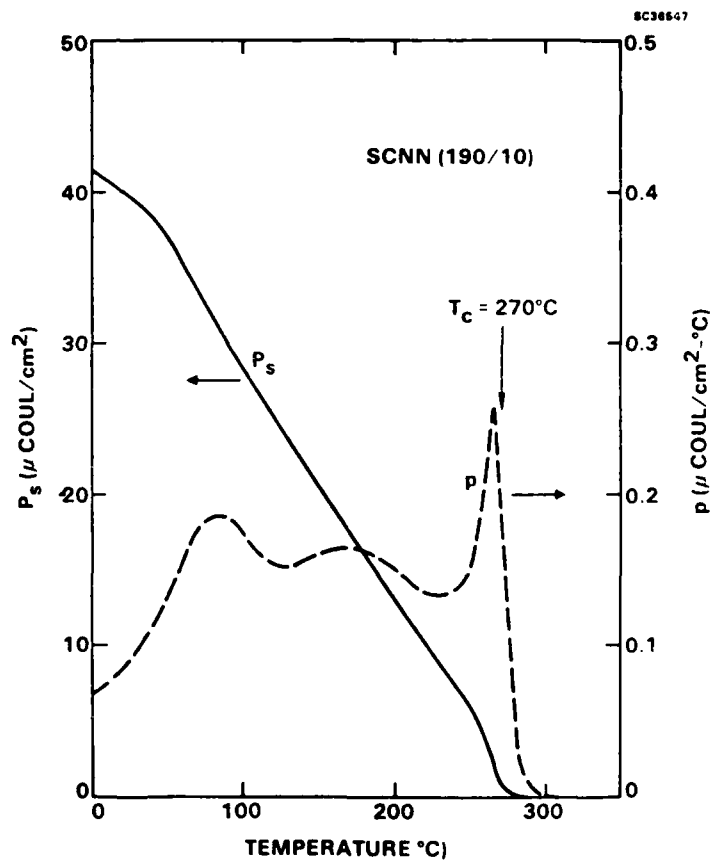
The room temperature dielectric constants for both crystallographic directions are nearly equal with a value of roughly 1700. However, a significant dielectric anisotropy is evident over a wide temperature range both above

and below room temperature. Our investigation of a number of ceramic compositions in the SCNN solid solution has shown that the degree of anisotropy at a given temperature can be tailored by variations in the amount of Ca substitution for Sr. In particular, the dielectric properties of the non- c axis directions such as $\langle 100 \rangle$, $\langle 110 \rangle$, etc., appear to be strongly affected by SCNN composition. This type of behavior is also observed for BSKNN crystals of differing compositions, e.g., BSKNN-1 and BSKNN-2 discussed in the next section.

The c -axis polarization and pyroelectric behavior of SCNN(190/10) as a function of temperature is shown in Fig. 7. Because of the presence of the second transition near 100°C , SCNN shows a relatively temperature-independent pyroelectric coefficient over a broad temperature range, unlike other tungsten bronze ferroelectrics which have a strongly decreasing pyroelectric coefficient below the ferroelectric phase transition temperature. As is typical of a high Curie point ferroelectric (270°C), the room temperature polarizability is large for this material at $40 \mu\text{coul}/\text{cm}^2$. This value is larger than for other well-known bronzes such as SBN, in part because of the added polarization arising from the second transition.

Fig. 7

Polarization and pyroelectric behavior of c -axis SCNN (190/10) as a functions of temperature





The high ferroelectric phase transition temperature of SCNN crystals (270°C) does not permit the use of oil bath poling procedures typically used with other ferroelectric materials. However, SCNN can be poled under high electric field conditions in a dry oxygen atmosphere without surface breakdown or excessive conduction and overheating problems. SCNN crystals have been successfully poled using dc electric fields of 6-10 kV/cm while cooling slowly through the ferroelectric phase transition. The electric field can be removed 30-40°C below the ferroelectric transition, since poling through the lower temperature ferroelastic transition does not significantly change the polarization at or below room temperature.

The large polarizability of SCNN, coupled with its large dielectric constants (1000-5000) and large anisotropy, implies a potential for very sensitive electro-optical, photorefractive and millimeter wave devices. In particular, longitudinal electro-optic effects should be very large because of the large non- $\langle 001 \rangle$ dielectric values, while also showing high response speed because of the relatively lower dielectric constant along the polar $\langle 001 \rangle$ axis, particularly below room temperature. Since SCNN appears to be ferroelastic at or below room temperature, it will be interesting to now examine the dielectric and electro-optic behavior of this material in the 30-90 GHz region, particularly in comparison with nonferroelastic bronzes such as BSKNN and SBN.

3.3.3 BSKNN Single Crystals

The $Ba_{2-x}Sr_xK_{1-y}Na_yNb_5O_{15}$ (BSKNN) solid solution exists on the $SrNb_2O_6$ - $BaNb_2O_6$ - $KNbO_3$ - $NaNbO_3$ quaternary system. Compositions within this system can possess either tetragonal or orthorhombic tungsten bronze crystal structures, the latter occurring for Na-content compositions such as $Sr_2NaNb_5O_{15}$ and $Ba_2NaNb_5O_{15}$. For this reason, the relative magnitudes of the transverse (r_{33}) and longitudinal (r_{51}) electro-optic coefficients are strong functions of both the Ba:Sr and K:Na ratios.

Our millimeter wave work on the BSKNN solid solution has focussed on BSKNN-1 ($Ba_{1.2}Sr_{0.8}K_{0.75}Na_{0.25}Nb_5O_{15}$) and more recently BSKNN-2 ($Ba_{0.5}Sr_{1.5}K_{0.5}Na_{0.5}Nb_5O_{15}$), both of which have been grown in single crystal form by the

Czochralski technique and have been extensively characterized at low frequencies (dc - 100 kHz) and at millimeter wave frequencies. Of these, BSKNN-2 has proven to be highly successful for the Czochralski growth of very high quality crystals of up to 1.5 cm cross section. The low frequency dielectric properties for this composition, shown in Fig. 8, are similar in overall behavior to those for BSKNN-1. However, BSKNN-2 has a lower Curie point (170-178°C), which contributes in part to its higher c-axis dielectric constant of 170 (poled) at room temperature, compared to 100-120 for BSKNN-1. The a-axis dielectric properties for BSKNN-2 are also considerably larger, with a low frequency dielectric constant of 750 at room temperature, rising to above 1000 at -150°C, values which are a factor of two or more greater than for tungsten bronze SBN:60 single crystals.

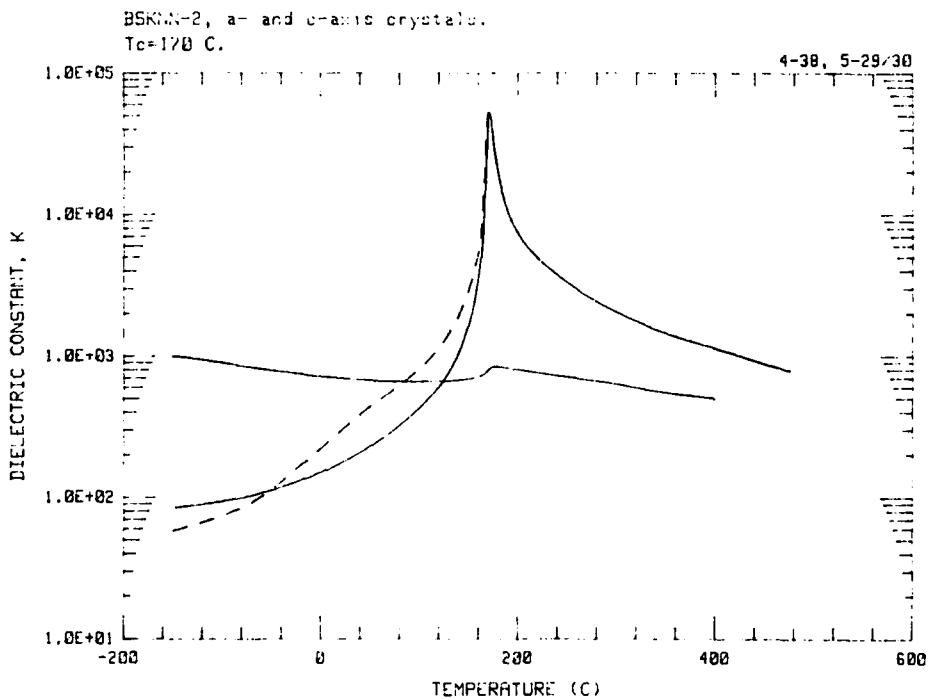


Fig. 8 Dielectric constant at 10 kHz for a- and c-axis BSKNN-2 single crystals poled at 10 kV/cm. Dashed curve is for thermally depoled c-axis crystal.



The c-axis polarization of BSKNN-2 as a function of temperature is shown in Fig. 9. Although BSKNN is a first-order phase transition ferroelectric, fluctuations in ionic site preference arising from the partially filled lattice structure result in a moderate distribution of transition temperatures in the crystal. Hence, the spontaneous polarization P_3 has a nonzero value at the mean Curie point, T_c , as seen in Fig. 9. Below T_c , the polarization rises sharply and attains a value of $34 \mu\text{C}/\text{cm}^2$ at room temperature, a value roughly equal to that for SBN:60. This high polarization, combined with the high a-axis dielectric constant, implies that BSKNN-2 should have a relatively large longitudinal (r_{51}) electro-optic coefficient at and below room temperature.

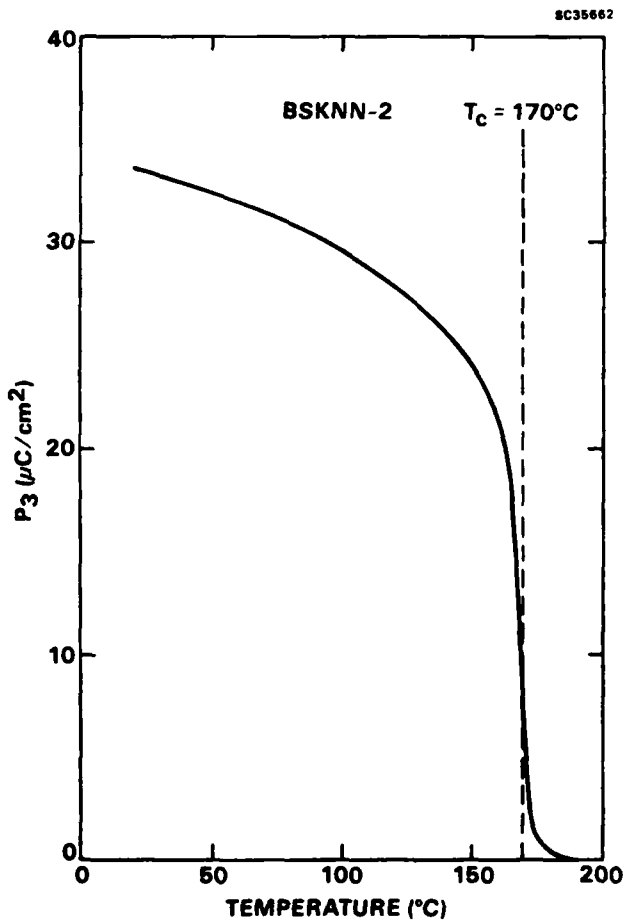


Fig. 9

Spontaneous polarization for c-axis BSKNN-2 as a function of temperature.



Rockwell International

Science Center

SC5345.AR

The BSKNN-2 values for dn_3/dE_3 at millimeter wave frequencies are anticipated to be much smaller than those for SBN:60 for temperatures at or below room temperature, since the c-axis dielectric constant of BSKNN-2 is relatively low. This has been confirmed experimentally and is discussed in Section 4.0. The values for dn_1/dE_3 over the same temperature range are anticipated to be comparable to those for SBN:60, particularly at 77K, since the a-axis dielectric constant of BSKNN-2 is comparatively larger and increases monotonically with decreasing temperature. However, the measured millimeter wave dn_1/dE_3 values for BSKNN-2 are found to be substantially lower than those for SBN:60, a highly surprising result. A more detailed discussion of these measurements and their implications is given in Section 4.0.



4.0 MILLIMETER WAVE MEASUREMENTS AND THEORETICAL MODELING

4.1 Introduction

Significant progress was made both in the development of advanced millimeter wave measurement techniques and in the determination of the nonlinear susceptibility of the BSKNN single crystal material system. The improvements achieved in measurement techniques allowed more accurate dielectric characterization to be carried out over wider frequency and temperature ranges. The data obtained by utilizing these new capabilities have resulted in more insights into the fundamental mechanisms controlling the dielectric response in the tungsten bronzes, as well as bringing closer to realization applications of these materials in practical device concepts. Advances made in theoretical modeling and device concept development as a consequence of this year's millimeter wave measurement effort are described separately in this report.

4.2 Millimeter Wave Dielectric Measurement Technique Development

Recent successes in the growth of large-sized, high quality single crystal BSKNN samples have made possible the application of free wave measurement techniques for determining the dielectric properties of samples at millimetered wave frequencies. As a consequence, much of the experimental difficulties associated with waveguide measurement techniques for high-dielectric materials such as (1) the need for an exact fit of samples to the inside dimensions of the waveguide to avoid the large errors associated with small residual gaps; (2) electrical isolation of the electrodes required to apply an external field to the sample from the waveguide walls; and (3) thermal insulation of the sample from the associated waveguide components for high and low temperature studies, can all be circumvented. Therefore, more direct determination of dielectric properties, which are less susceptible to systematic sources of errors, can be made with free wave methods over wider temperature and frequency ranges.

A typical arrangement of the experimental apparatus used for the free space measurements for each wavelength band is shown in Fig. 10. A spot-focusing lens antenna with an f-number of unity and a diameter of 15.25 cm is

used to focus a linearly polarized microwave signal onto a planar sample positioned at the focal point. The spot size achievable is nearly diffraction-limited and is approximately 1.5 cm at 35 GHz and 0.4 cm at 130 GHz. The lens antennas typically have a working bandwidth of 10 GHz and instrumentation is currently available to almost completely cover the frequency range 35 - 135 GHz (33 - 50 GHz, 55 - 65 GHz, 90 - 135 GHz).

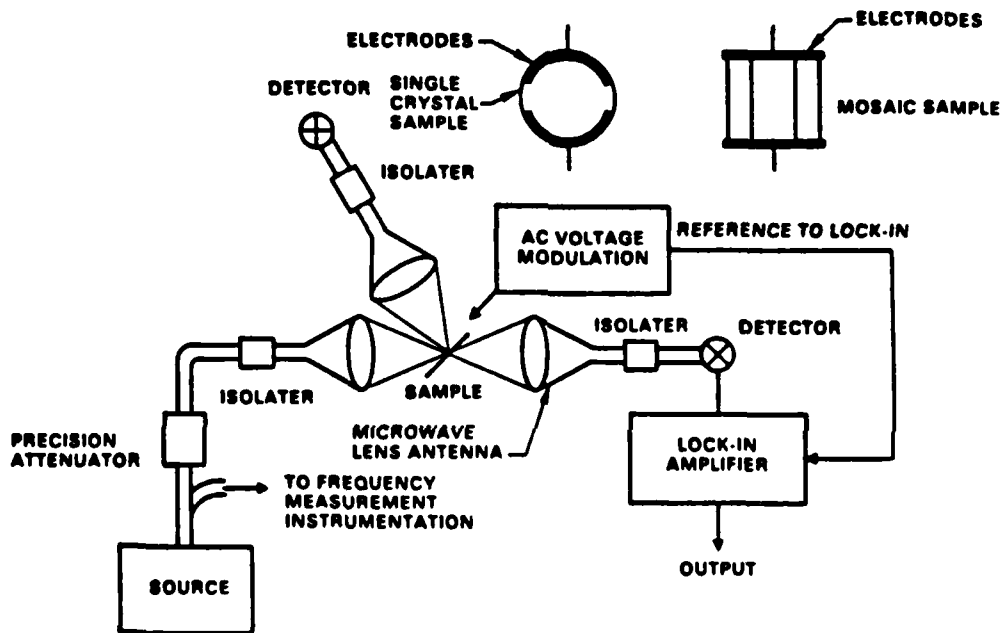


Fig. 10 Schematic of the free-space millimeter wave dielectric characterization apparatus.

The samples used are either a single crystal suitably cut along the desired crystal axis or a mosaic of individual single crystal sections. For BSKNN, sets of three rectangular sections of identical dimensions cut along the crystal c-axis from adjacent portions of a single crystal boule were used to assemble mosaic structures with approximate dimensions of 2 cm x 2 cm. Platinum electrodes were then deposited on the opposite edges of the sample across the crystal c-axis. The electrodes were used to both initially pole the samples and to apply the necessary external electric field for the nonlinear susceptibility (dn/dE) measurements. The mosaic was sufficiently large to satisfy the size



requirements for the free wave measurement method over the entire range of frequencies studied.

The samples were positioned at a given incidence angle in the path of the microwave beam, and their transmission and reflection coefficients were measured by two additional identical antennas suitably aligned with respect to the incident beam and the sample. The dielectric constant and dielectric loss were then deduced from these observed reflection and transmission coefficients as a function of frequency for a given sample thickness and orientation. For low temperature studies, the sample is placed in an enclosure with thin polyethylene windows (0.02 cm) and the enclosure is then filled with a cryogenic fluid (liquid nitrogen). Dry nitrogen is used to purge the outsides of the windows to prevent moisture condensation, and the measurement is made through the window and the liquid nitrogen surrounding the sample. Because of the low dielectric constant and low loss properties of LN₂ and the window material compared to those for BSKNN, the effects of these materials on the observed reflection and transmission coefficients of the sample are found to be minimal.

The nonlinear dielectric response (dn/dE) of the sample was determined by applying an alternating bias voltage to the electrodes and measuring the amplitude modulation component of the transmitted and reflected millimeter wave intensities. The magnitude of dn/dE was then computed from the required change in the millimeter wave index of refraction to match the observed changes in the respective transmission and reflection coefficients. When the applied voltage along the crystal c-axis is colinear with the millimeter wave electric field vector, the measurement yields dn_3/dE_3 , while a 90° rotation of the beam polarization yields dn_1/dE_3 .

4.3 Millimeter Wave Dielectric Properties of Single Crystal BSKNN

The dielectric properties of single crystal BSKNN-2 samples were determined at 33 - 50 GHz and 125 - 135 GHz using the described free wave measurement method. These included both crystal orientations at room and liquid nitrogen temperatures. The dielectric constant and loss were determined by fitting the observed reflection and transmission coefficient data to theoretical expressions



for plane wave propagation through a dielectric slab of given thickness. The validity of the data reduction procedure and self-consistency in the results were verified by performing the measurements for two sample thicknesses at various angles of observation. Typical data obtained between 33 - 50 GHz for a BSKNN-2 sample of 0.0445 cm are shown for illustrative purposes in Figs. 11 and 12. The measured room temperature c-axis reflection coefficients at a 30° angle and transmission coefficients at a 10° angle are shown together with the best-fit computed results (solid lines) for $\epsilon' = 95$, $\epsilon'' = 18$. The agreement is seen to be excellent throughout the frequency range shown. The measured c-axis reflection coefficients at liquid nitrogen temperature and the a-axis reflection coefficients at room temperature, both taken at 30° incidence angle, are shown in Figs 13 and 14. Again, good fits are obtained with the theoretical expressions using dielectric constant values of $\epsilon' = 39$, $\epsilon'' = 2$ and $\epsilon' = 427$, $\epsilon'' = 81$, respectively.

The measured dielectric properties for the BSKNN-2 samples studied are summarized in Table 3. In general, somewhat larger values for both the dielectric constant and the dielectric loss are found for these samples when compared to previous values obtained in last year's study. This most likely reflects differences in composition. The large dependence of c-axis loss on temperature is again confirmed, as is the almost complete independence of a-axis properties on temperature. Moreover, the observed dielectric properties are only weakly dependent on frequency over the range of observation, with the results at 130 GHz showing only a slight decrease in the dielectric constant and a somewhat larger increase in the dielectric loss.

SC5345.AR

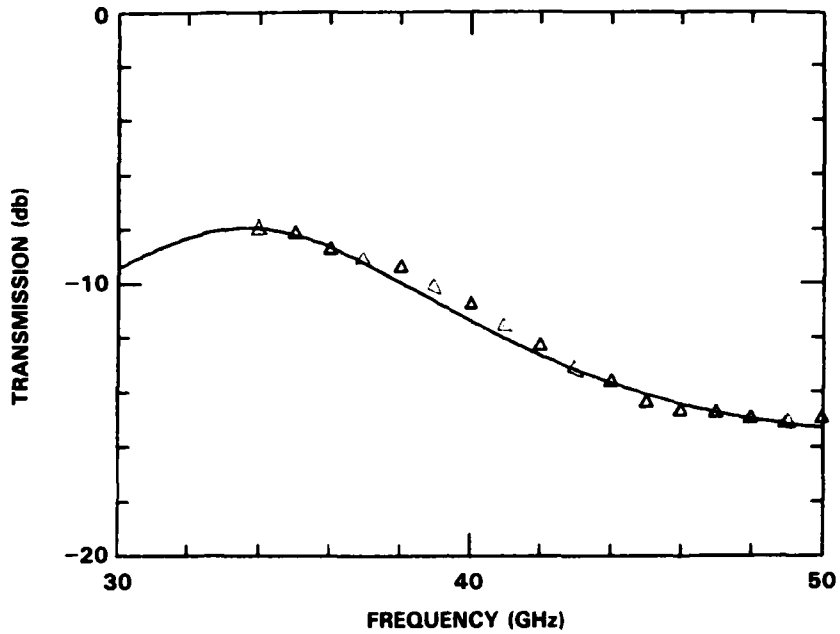


Fig. 11 33-50 GHz transmission of c-axis BSKNN-2 at room temperature.
 $t = 0.0445$ cm.

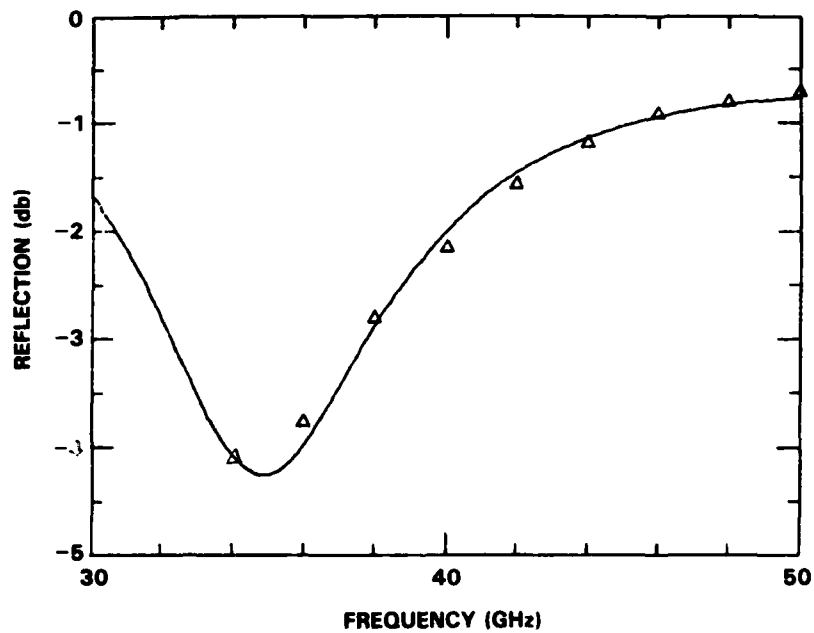


Fig. 12 33-50 GHz reflection of c-axis BSKNN-2 at room temperature.



SC5345.AR

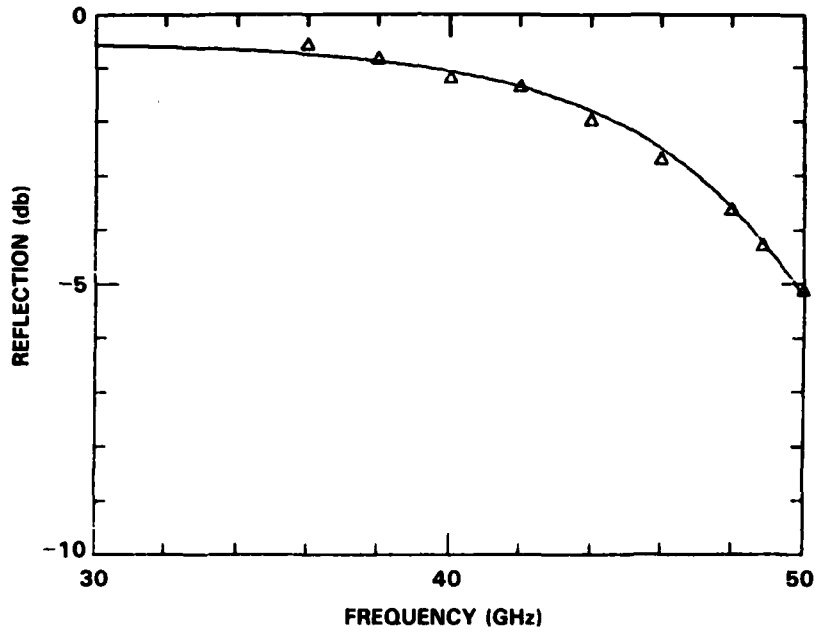


Fig. 13 33-50 GHz reflection of c-axis BSKNN-2 at 77K.

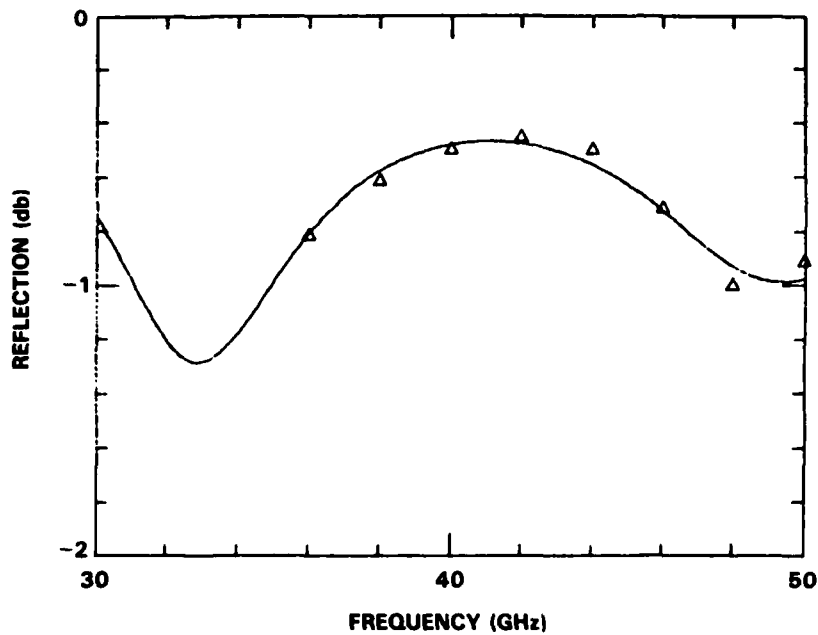


Fig. 14 33-50 GHz reflection of a-axis BSKNN-2 at room temperature.



Table 3
Millimeter Wave Dielectric Properties of Single Crystal BSKNN-2

	Frequency (GHz)	Temperature (K)	ϵ'	ϵ''	$\tan \delta$	dn_i/dE_j (m/V) ^j
c-axis	33 - 50	295	95	18	0.19	$dn_3/dE_3 = 4.2 \times 10^{-7}$
		77	39	2	0.05	$dn_3/dE_3 = 4.3 \times 10^{-8}$
a-axis	33 - 50	295	427	81	0.19	$dn_1/dE_3 = 5 \times 10^{-8}$
		77	418	70	0.17	$dn_1/dE_3 = 3 \times 10^{-8}$
c-axis	125 - 135	295	93	26	0.28	$dn_3/dE_3 = 4.6 \times 10^{-7}$
		77	36	2.5	0.07	$dn_3/dE_3 = 4 \times 10^{-8}$
a-axis	125 - 135	295	430	80	0.9	--

The nonlinear susceptibility coefficients dn_3/dE_3 and dn_1/dE_3 were determined at room temperature and at liquid nitrogen temperature by measuring the amplitude modulation of the reflected and transmitted millimeter wave signal caused by an applied AC voltage across the sample c-axis. This modulation signal is essentially proportional to the derivative of the reflection and transmission spectra, and has maximum sensitivity when the slope of the respective curves are largest. For instance, as shown in Figs. 11 and 12 for the case of c-axis properties at room temperature, the slopes are greatest at approximately 40 GHz. Consequently, the measurements are carried out for this case in this frequency region. Tests were also performed to verify the dependence of the modulation signal on the applied field strengths and the frequency of modulation. As expected, the modulation was found to be linearly proportional to the applied voltage up to the maximum value of 2500 V ($E = 1.2 \times 10^5$ V/m) and is independent of modulation frequency over the available range of 100 Hz to 20 KHz for all cases studied. In addition, agreement was obtained between the values for dn/dE deduced from the transmission and reflection data, indicating good internal self-consistency in the results.



SC5345.AR

The data obtained for the dn/dE coefficients are shown in Table 3. The room temperature value for dn_3/dE_3 is approximately 4×10^{-7} m/V and is essentially independent of frequency over the range studied within the experimental uncertainty. This value drops to approximately 4×10^{-8} m/V at liquid nitrogen temperature, but is accompanied by a corresponding decrease in the dielectric loss in the material of approximately the same order of magnitude. Consequently, the figures of merit in potential device applications are approximately the same. The nonlinear coefficient dn_1/dE_3 is $\sim 5 \times 10^{-8}$ m/V and decreases slightly with temperature. This is not surprising since the dielectric properties along the crystal a-axis were also found to be relatively insensitive to temperature.

Compared to the results previously obtained for SBN in last year's effort, the nonlinear coefficients for BSKNN are substantially lower. For instance, the values for dn_3/dE_3 in SBN:60 are in the range $2 - 3 \times 10^{-6}$ m/V at room temperature and 5×10^{-7} m/V at liquid nitrogen temperature, which are $\sim 10 - 20X$ larger than the values found for BSKNN. However, the dielectric losses in SBN:60 are also substantially higher. When absorptions are taken into account for these two materials in device applications, BSKNN compares favorably with SBN, particularly at low temperatures. Consequently, both materials show promise and further developmental effort should be carried out to optimize dn/dE and to reduce the millimeter wave loss.

4.4 Progress Summary of Experimental Effort at UCLA

Recent advances in millimeter wave systems call for new control devices with low losses and high power capability. Electro-optic modulators and beam steerers could fill this need if suitable materials can be found for the active components. Our study has focussed on two promising ferroelectric materials in the tungsten bronze family, SBN and BSKNN. Previously we reported low millimeter wave losses in these materials at low temperatures for a particular geometry. Over the past year, further measurements of the temperature dependence of absorption and refraction have been made, and measurements have begun on the temperature dependence of the transverse electro-optic effect.



SC5345.AR

Our 55 - 110 GHz millimeter wave spectrophotometer system has been modified to allow detection of incident and reflected powers, and thereby give more accurate determinations of the sample properties. The sample mounting technique has also been changed to provide greater thermal conductance, and so more uniform temperatures and a lower minimum temperature (20K) are obtained. Figures 15 and 16 summarize the measurements of the refractive index n and the absorption index k for SBN (circles) and two compositions of BSKNN (triangles and squares). Geometries with the a -axis (open symbols) and the c -axis (closed symbols) parallel to the radiation electric field are shown. The huge anisotropies observed may be understood in terms of coupling to small oscillations in the orientation of the distorted oxygen octahedral configurations present in these materials. These results have been reported in the literature.¹

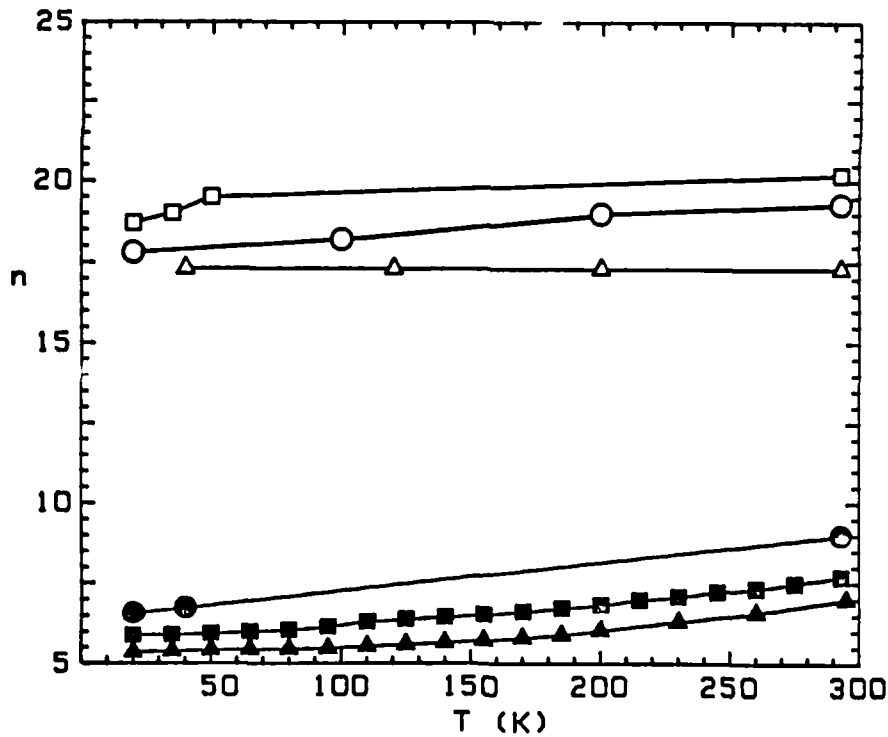


Fig. 15 55-110 GHz refractive index n as a function of temperature for SBN:60 (circles), BSKNN-1 (triangles) and BSKNN-2 (squares). Open symbols are for the a -axis, closed for the c -axis.



SC5345.AR

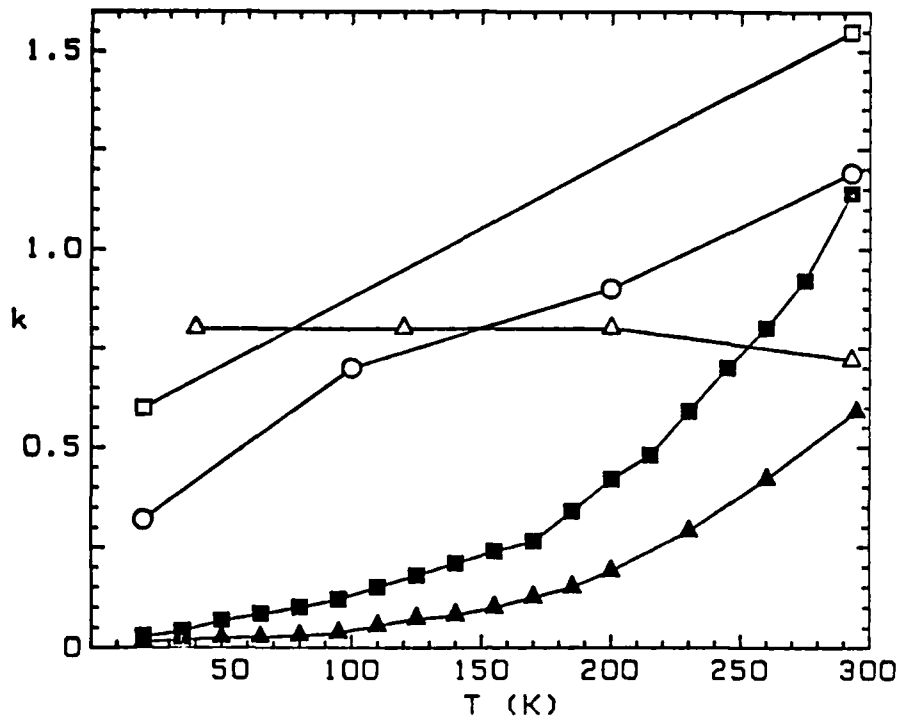


Fig. 16 55-110 GHz absorption index k as a function of temperature for SBN:60 (circles), BSKNN-1 (triangles) and BSKNN-2 (squares). Open symbols are for the a-axis, closed for the c-axis.

Transverse electro-optic measurements require a sample mounting arrangement different from that used for measurements requiring no applied field, i.e., where the sample is sandwiched between waveguide flanges, since the metal flanges divert the field lines. A free space mounting geometry is necessary, with diffraction minimized by using a sample of large transverse area between two closely-spaced waveguide horns. The sample temperature is controlled by contacting its face to a BeO ceramic plate which contacts, around its edges, a copper cold finger. This system employs a closed-cycle refrigerator, diode sensor and heater for temperature stabilization, and Brewster angle vacuum windows as described previously.

Figure 17 shows the effect of a large DC applied voltage on the room temperature spectrum of BSKNN in the (333) geometry. The spectral independence indicates that the change in transmittance is due to the combined effect of both a Fresnel reflection coefficient change and a shifting of the sample's Fabry-Perot peaks. One of these peaks is seen as the envelope function for several

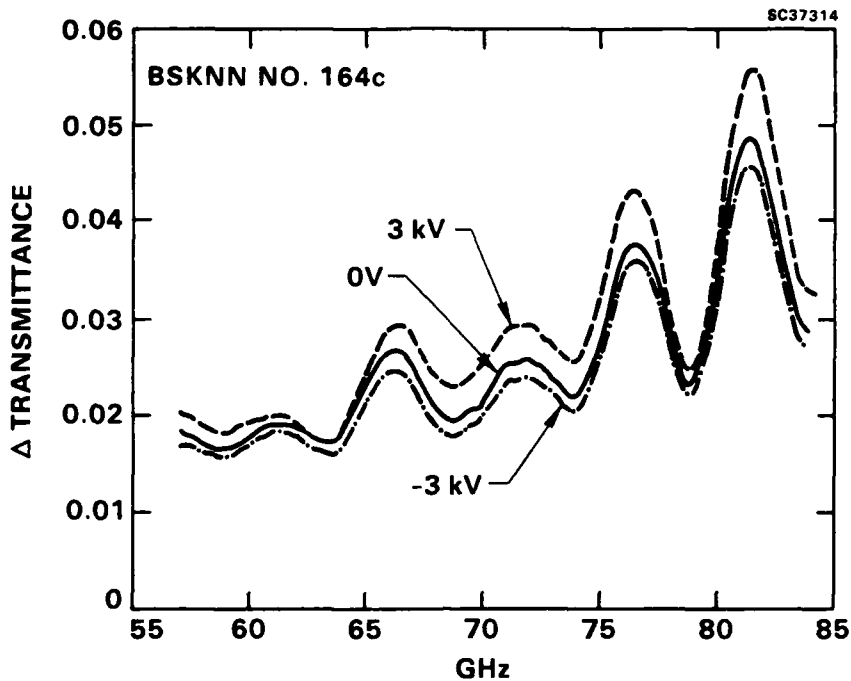


Fig. 17 Transmittance as a function of frequency and applied DC voltage for BSKNN at room temperature.

narrower peaks which do not shift because they are due to extraneous standing waves outside the sample.

More accurate measurements can be made using an AC applied voltage and a fast response diode detector input to a lock-in amplifier. Figure 18 shows the change in transmittance for BSKNN measured this way. The polar nature of the Pockels effect is clearly shown here when the voltage is reversed. The analysis of these curves is complicated by the effects of diffraction and extraneous standing waves; but for the present, rough estimates are readily made of the change in refractive index n per applied field E , given by

$$\frac{\Delta n}{\Delta E} = \frac{1}{2} n_e^3 r_{33} \quad (4.1)$$

where r is the Pockels tensor. For BSKNN at room temperature, this value is estimated as 1.4×10^{-6} m/V. The transmittance change for SBN is shown in



SC5345.AR

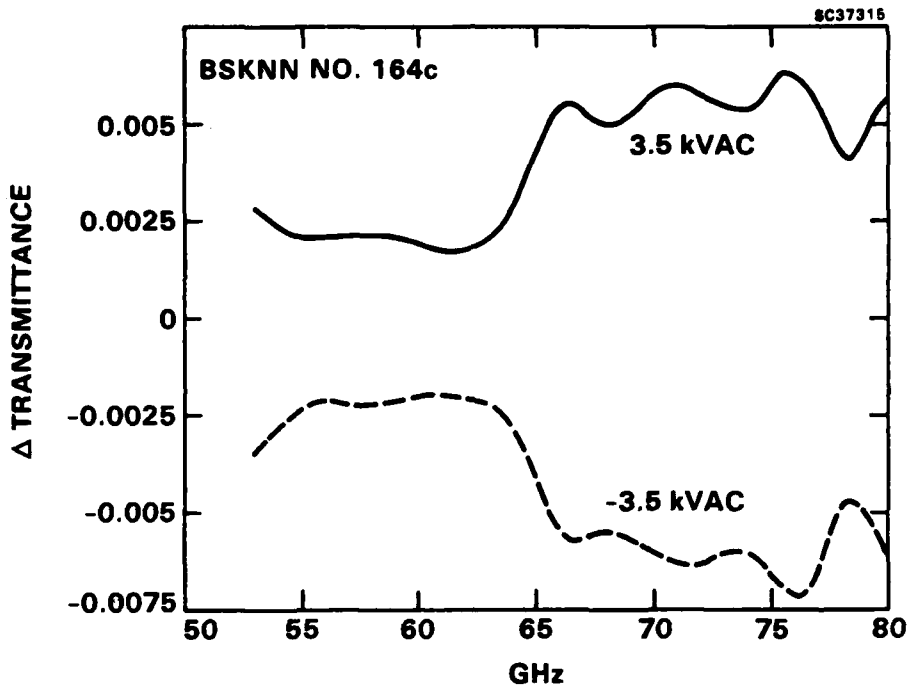


Fig. 18 Transmittance change as a function of frequency for BSKNN at 3.5 kV at room temperature.

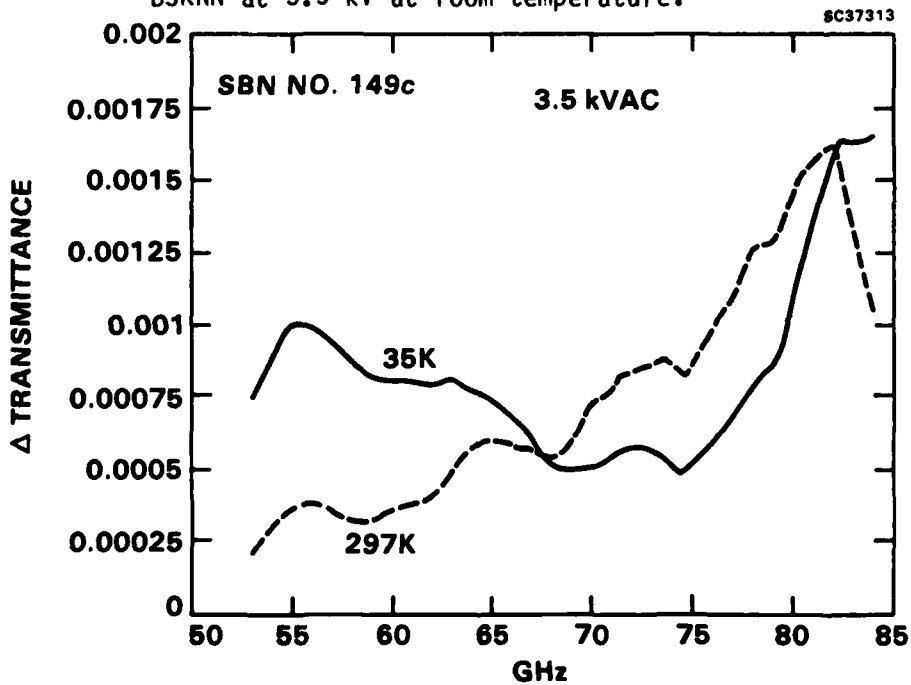


Fig. 19 Comparison of transmittance change for SBN:60 at 3.5 kV at 35 and 297K.



Fig. 19 The room temperature measurements of $\Delta n/\Delta E \sim 8 \times 10^{-7}$ m/V is consistent with other reported values;² while the low temperature value at 35K decreases to about 4×10^{-7} m/V.

A figure-of-merit (FOM) relevant for comparison of material properties is given as

$$\text{FOM} = \frac{n_e^2 r_{33}^2}{k} = \frac{2}{n_e k} \left[\frac{\Delta n}{\Delta E} \right] \quad (4.2)$$

Using our measured parameters, we find that the FOM for SBN improved by a factor of roughly 40 at low temperature. Such an improvement makes SBN at low temperature comparable in performance to BaTiO₃ at room temperature,³ while avoiding the practical difficulties associated with BaTiO₃.⁴

In future work, we plan to continue our transverse electro-optic measurements and to refine our analysis of the data. Next, the longitudinal electro-optic effect in SBN and BSKNN will be investigated.

4.5 Theoretical Modeling

4.5.1 Dielectric Permittivity and Loss

Ferroelectric materials exhibit a variety of unusual effects connected with their structural phase transitions. The interrelations among these effects have been well accounted for in the phenomenological free energy models of Landau, Ginsberg and Devonshire. Combining such a model with the soft-mode description of the ferroelectric phase transition leads to a prediction for the frequency dependence of ferroelectric properties such as dielectric permittivity, loss tangent, and electric field sensitivity. It has been a primary thrust of our investigations over the past five years to test these predictions for a particular class of ferroelectrics, the tungsten bronzes, at millimeter wave frequencies.

In our laboratory, considerable effort has been devoted to developing growth techniques for tungsten bronze ferroelectrics, and single crystals of large size are now available for several different compositions. Our millimeter wave



SC5345.AR

dielectric measurements are being carried out primarily on the various compositions of barium strontium potassium sodium niobate (BSKNN) and strontium barium niobate (SBN).⁵

The relative dielectric permittivity (ϵ'/ϵ_0) and loss (ϵ''/ϵ_0) for two compositions of BSKNN and SBN are summarized in Table 4 for room temperature (295K) and liquid nitrogen temperature (77K). Measurements were made at various frequencies above 30 GHz as noted in the table. In obtaining these results, waveguide transmission and reflection on samples filling the guide were used below 50 GHz, while free space measurements of reflected and transmitted power were used above 90 GHz.

Table 4
Millimeter Wave Dielectric Properties of Single Crystal BSKNN and SBN

Axis	Temperature (K)	BSKNN-2*		SBN:60 [†]		Frequency
		ϵ'/ϵ_0	ϵ''/ϵ_0	ϵ'/ϵ_0	ϵ''/ϵ_0	
c	295	95	18	158	86	30 - 50 GHz
	77	39	2	124	8.8	
a	295	427	81	231	51	BSKNN: 125-135 GHz
	77	418	70	190	37	
c	295	93	26	273	149	SBN: 90-100 GHz
	77	36	2.5	67	23	
a	295	430	80	211	37	
	77			180	29	

*Ba_{0.5}Sr_{1.5}K_{0.5}Na_{0.5}Nb₅O₁₅

[†]The low and high frequency samples of SBN:60 are from two different growths. Large boule-to-boule variations in permittivity have been found.

The features common to all the ferroelectrics we have studied include:

1. A large decrease in polar axis permittivity from its dc value.
2. A large polar axis dielectric loss.



3. A large temperature dependence of these properties.
4. Perpendicular to the polar axis, the loss is smaller at room temperature but remains high on cooling.

This behavior is generally not predicted by the soft-mode model, and suggests that a millimeter wave relaxation mechanism is responsible for a majority of the observed dc polarizability along the polar axis.

We have considered in some detail a model based on the notion that there is substantial variation in the direction and magnitude of the spontaneous polarization within a poled single crystal, probably as a result of the microscopic variations in composition which arise naturally in solid solution systems. Experimental evidence for such departures from uniform polarization can be found in the recent publications of Burns and Dacol.⁶

To obtain a qualitative understanding of the predictions of this model, we have calculated the polar axis microwave loss for an array of microdomains of reversed polarization scattered throughout the crystal. Essentially, the microwave electric field does mechanical work on the charge trapped at the domain walls, which shows up in the form of damped acoustic waves in the crystal. A similar model for polydomain loss has been proposed by Turik and Shevchenko.⁷ We do not assume any field-induced reversal of the local polarization.

The resulting form of the microwave loss can be presented schematically as

$$\epsilon'' = [2Q(\epsilon' - \epsilon_0)P_0]^2 c^P \left(\frac{d_0}{s}\right) \langle f(\omega d/v, \omega\eta) \rangle_d, \quad (4.3)$$

where Q is the appropriate electrostriction constant for a particular orientation of the applied field, c^P is the appropriate elastic modulus, P_0 is the spontaneous polarization, d_0 is the average domain size along the polar axis, s is the inverse of the number of domain walls per unit length, v is the sound velocity for longitudinal acoustic waves, and η is the elastic damping for these waves. The resonance function, f , has a complicated structure which, on average-



ing over domain size, reduces to the Debye relaxor form at low and high frequency, with a relaxation time given by $\tau = d_0/v$.

For the simplest geometry, i.e., stripe domains spaced along the polar axis, the electrostrictive force per unit area on each domain wall is $F_{33} = 2Q_{33} c_{33}^p (\epsilon_{33} - \epsilon_0) P_0 E_3$, where E_3 is the microwave electric field parallel to the polar axis. The electrical power dissipated into acoustic waves in a domain of half-width, d , is found from the elastic equations of motion to be

$$\dot{W} = -\text{Im} \left\{ \frac{2(F_{33})^2}{\rho\omega} \frac{k \tan kd}{1 - i \tan kd} \right\} \quad (4.4)$$

where $k = p + iq$ is the complex wave number for the longitudinal acoustic wave of frequency ω along the polar axis and ρ is the crystal mass density. Equating this dissipation summed over all domains to the resistive loss $\text{Re}(\mathbf{J} \cdot \mathbf{E})$ throughout the crystal volume gives the formula (4.3), with

$$f(\omega d/v, \omega\tau) = \frac{pd[(\tan pd)^2 + \tanh qd] + qd \tan pd (1 - \tanh qd)}{(1 + \tanh qd) [1 + (\tan pd)^2]} (\omega d/v)^2 \quad (4.5)$$

Here $p = \omega/v$ and $q = \omega\tau/2\rho v^2$.

For small kd (low frequency limit), the loss function, f , is proportional to ω . For large kd , $\tanh qd$ tends to unity, so f becomes proportional to ω^{-1} . At intermediate values of kd , the loss function passes through a series of damped oscillations with peaks at the piezoelectric resonances. Averaging the loss function over a range of domain sizes, d , tends to wash out these resonances, giving a form for the loss which is close to the Debye relaxor: $\omega\tau/(1 + \omega^2\tau^2)$.

If the assumed microscopic variations in crystal composition cause local tilting of the spontaneous polarization, then there will be a similar acoustic loss for microwave electric fields oriented perpendicular to the (average) polar axis. A unique feature of this loss mechanism is that it would be effective independent of whether the local P_0 is "up" or "down," and, therefore, the loss should not show a decrease with temperature due to progressive ordering of the local polarization.



A significant qualitative feature of this loss model is the scaling of the loss ϵ'' with the square of the high-frequency permittivity. Table 5 shows the behavior of this ratio for three tungsten bronze crystals at 30 - 50 GHz. One should note particularly that the two BSKNN compositions have identical ratios at a given temperature, although the absolute values of ϵ'' differ by a factor of two. The trend in these ratios with temperature is also interesting, and suggests that the number of reversed domains is increasing as $(T_c - T)^{-2}$ as the Curie temperature is approached.

Table 5
Trends in Polar Axis Loss Ratio $\epsilon_0 \epsilon'' / (\epsilon')^2$ at 30 - 50 GHz
Compared with Acoustic Loss Model

	BSKNN-1	BSKNN-2	SBN:60
Room T	2.2×10^{-3}	2.0×10^{-3}	3.4×10^{-3}
Liquid N ₂	1.2×10^{-3}	1.3×10^{-3}	0.6×10^{-3}
Variation with Temperature			
RT/LN ₂	1.8	1.5	5.7
$(T_c - LN_2) / (T_c - RT)$	2.2	2.5	5.1

The actual magnitude of the millimeter wave loss, as derived from this expression for the tungsten bronzes, is too small by about a factor of three to account for the observed dispersion. However, the trends are very suggestive, and it is reasonable to expect that extending the model to include polarization reversal will yield better quantitative agreement.

4.5.2 Electric Field Sensitivity

Polarized ferroelectrics exhibit a linear dependence of their dielectric permittivity ϵ' or refractive index n on applied dc electric field strength, arising from the additional polarization induced by the field. Very few measurements of this effect have been made at millimeter wave frequencies since the early work of Boyd, et al.⁸ Klein⁹ has examined lithium niobate and, more recently, barium titanate. We have made measurements over a range of fre-



quencies on SBN:60 as samples of sufficient size became available from our materials development research, and more recently we have measured BSKNN-2 between 125 and 135 GHz.

A summary of the polar axis sensitivity, dn_3/dE_3 , for these two materials is given in Table 6. The generalization of Miller's rule proposed by Boyd,⁸ which states that dn/dE should be proportional to n^5 , appears to work well in comparing the room temperature and 77K values of dn/dE for BSKNN-2, but not well at all for SBN:60. It will be interesting to see how other tungsten bronzes fit this scheme. For most device applications of this effect, one seeks both large sensitivity and low loss, and reliable guidelines for the selection of appropriate materials for growth would greatly benefit this work.

Table 6
Electric Field Sensitivity of the Polar Axis Refractive Index at 100 GHz

	BSKNN-2 dn/dE	n	SBN:60 dn/dE	n
Room T	4×10^{-7} m/V	9.8	1.6×10^{-6} m/V	17.1
Liquid N ₂	4.3×10^{-8} m/V	6.25	5.0×10^{-7} m/V	8.3
Comparison with Boyd's Rule				
dn/dE(RT/LN ₂)	9.3		3.2	
(n _{RT} /n _{LN₂})	9.5		37	

A useful figure-of-merit defined by Klein⁹ is related to the phase shift accumulated over a single absorption length, λ , per volt/meter of applied field: $d\phi_\lambda/dE = k_0\lambda(dn/dE)$. Combining Boyd's rule with our millimeter wave loss model, we find

$$d\phi_\lambda/dE \propto n^2 \quad (4.6)$$



Rockwell International
Science Center

SC5345.AR

Thus, within a single class of materials such as the BSKNN solid solution system, one should expect that the device utility will scale with $n^2 = \epsilon'$, the millimeter wave polarizability.



5.0 CONCLUSIONS AND RECOMMENDATIONS

The factors controlling millimeter wave loss in ferroelectrics are now emerging, as evidence accumulates from our studies of the temperature and composition dependence in the tungsten bronzes, and from microstructural characterization of other solid solution systems (Chan & Harmer).¹⁰ Polarization is not uniform, but varies due to microscale compositional fluctuations, providing a means by which the millimeter wave electric field can put energy into the acoustic modes of the crystal. Fortunately, this loss does not grow as fast with increasing permittivity as does the electric field sensitivity dn/dE along the polar axes. We thus have identified a route to obtain the basic device function - phase modulation - with tolerable loss, by moving within the tungsten bronze family toward the highest permittivity compositions.

Our materials growth efforts over the past year have, in fact, been directed toward higher permittivity. PBN doped with La^{3+} was prepared as a grain-oriented ceramic; small crystals of SCNN were grown by the Czochralski technique; and new BSKNN compositions were prepared by sintering. In addition, we found that La doping of SBN:60 or :75 dramatically increases the permittivity and other ferroelectric properties. SBN:60 crystals of 2 cm diameter with La doping have now successfully been grown, and they will be characterized at millimeter wave frequencies in the near future.

Our successful development of growth techniques for the various types of tungsten bronzes, coupled with our improved knowledge of the interrelationship of the materials properties within this family, now provides an opportunity for both developing a fundamental understanding of mechanisms and exploiting properties of the bronzes in various device concepts.



6.0 FUTURE PLANNED RESEARCH

The investigation of factors controlling the high frequency response in selected high-dielectric and electro-optic materials will be continued. This effort will include the continued development of Czochralski and hot-pressing growth techniques and the measurement of material dielectric properties at frequencies up to 140 GHz. Special emphasis will be placed on morphotropic phase boundary crystals or ceramics, where both the dielectric and electro-optic properties are exceptionally large, with the goal of maintaining large millimeter wave dn/dE and low absorption over a wide range of temperatures. The following specific tasks are to be addressed in the coming year:

1. Establish the hot-pressing technique for morphotropic phase boundary tungsten bronze $Pb_{1-x}Ba_xNb_2O_6$, $Ba_{2-x}Sr_xNaNb_5O_{15}$, $Pb_{2-x}Sr_xNaNb_5O_{15}$, etc. and perovskite, PLZT, PZT, $Pb_{1-x}Bi_x(Ti_{1-x}Fe_x)O_3$, etc.
2. Further establish the bulk single crystal growth of $Sr_{0.75}Ba_{0.25}Nb_2O_6$ (SBN:75) and a few other promising bronze compositions by the Czochralski technique.
3. Low temperature studies: Measurements of high frequency permittivity down to 77K will be extended to a variety of ferroelectrics, including MPB compositions, SBN:75, and a few other ferroelectric crystals.
4. The variation of the millimeter wave electro-optic response (dn/dE) with temperature will be investigated down to 77K for MPB compositions, SBN:75, BSKNN and other available materials.
5. Continued development of theoretical models for the observed millimeter wave temperature-dependent dielectric and electro-optic properties.



**Rockwell International
Science Center**

SC5345.AR

6. At UCLA, the design and laboratory measurement of millimeter wave modulators based on ferroelectrics from this program will be continued. Also, device concepts and figure-of-merit will be evaluated based on current results.



7.0 PUBLICATIONS AND PRESENTATIONS

7.1 Publications

1. B. Bobbs, M. Matloubian and H.R. Fetterman, "Millimeter Wave Absorption and Refraction in Tungsten Bronze Ferroelectrics," Appl. Phys. Letts. 48(29), 1642 (1986).
2. L.E. Cross and R.R. Neurgaonkar, "A Phenomenological Analysis of Tetragonal Tungsten Bronze Ferroelectrics," submitted to J. Materials Science.
3. R.R. Neurgaonkar, W.K. Cory and J.R. Oliver, "Growth and Properties of Ferroelectric Tungsten Bronze $K_3Li_2Nb_5O_{15}$ Crystals," submitted to J. Cryst. Growth.
4. R.R. Neurgaonkar, W.W. Ho, W.K. Cory, W.F. Hall and L.E. Cross, "Low and High Frequency Dielectric Properties of Ferroelectric Tungsten Bronze $Sr_2KNb_5O_{15}$ Crystals," Ferroelectrics 51, 185 (1984).
5. B. Bobbs, M. Matloubian, H.R. Fetterman and R.R. Neurgaonkar, "Electro-optic Devices for Millimeter Waves Using Cooled Ferroelectrics," SPIE 545, 35 (1985).
6. W.W. Ho, W.F. Hall and R.R. Neurgaonkar, "Millimeter Wave Dielectric Properties of Single Crystal Strontium Barium Niobate at Cryogenic Temperatures," Proc. 10th Int'l Conf. on IR and Millimeter Waves, Lake Buena Vista, FL (1985).
7. W.F. Hall, W.W. Ho, R.R. Neurgaonkar and W.K. Cory, "Millimeter Wave Dielectric Properties of Tungsten Bronze Ferroelectrics at 77 and 300K," accepted for publication in the IEEE Proc. of the International Symposium on Applications of Ferroelectrics (ISAF) Lehigh U. (1986).
8. J.R. Oliver, R.R. Neurgaonkar and G.L. Shoop, "Structural and Ferroelectric Properties of Morphotropic Phase Boundary Systems in the Tungsten Bronze Family," accepted for publication in the IEEE Proc. ISAF, Lehigh U. (1986).
9. W.F. Hall, W.W. Ho, R.R. Neurgaonkar and J.R. Oliver, "Model for Millimeter Wave Properties of Tungsten Bronze Ferroelectrics," to be submitted to the J. Appl. Phys.



7.2 Presentations

1. R.R. Neurgaonkar, "Growth and Applications of Tungsten Bronze Family Crystals for Optoelectronic Applications," presented at the Society of Photo-Optical Instrumentation Engineers 19th Annual International Technical Symposium, San Diego, CA, (1985).
2. R.R. Neurgaonkar, "Epitaxial Growth of Ferroelectric Films for Optoelectronic Applications," presented at the 6th International Meeting on Ferroelectricity, Kobe, Japan (1985).
3. W.W. Ho, W.F. Hall and R.R. Neurgaonkar, "Millimeter Wave Dielectric Properties of Single Crystal Strontium Barium Niobate at Cryogenic Temperatures," presented at the 10th Int'l Conf. on IR and Millimeter Waves, Lake Buena Vista, FL (1985).
4. J.R. Oliver, R.R. Neurgaonkar, W.K. Cory, W.F. Hall and W.W. Ho, "Tungsten Bronze Materials for High Frequency Dielectrics," presented at the 88th Annual Meeting of the American Ceramic Soc., Chicago, IL (1986).
5. W.F. Hall, W.W. Ho, R.R. Neurgaonkar and W.K. Cory, "Trends in High Frequency Dielectric Properties of Tungsten Bronze Ferroelectrics," presented at the 88th Annual Meeting of the Am. Ceramic Soc., Chicago, IL (1986).
6. W.F. Hall, W.W. Ho, R. R. Neurgaonkar and W.K. Cory, "Millimeter Wave Dielectric Properties of Tungsten Bronze Ferroelectrics at 77 and 300K," presented at the IEEE Int'l Symposium on Applications of Ferroelectrics (ISAF), Lehigh U. (1986).
7. J.R. Oliver, R.R. Neurgaonkar and G.L. Shoop, "Structural and Ferroelectric Properties of Morphotropic Phase Boundary Systems in the Tungsten Bronze Family," presented at the IEEE-ISAF, Lehigh U. (1986).



8.0 REFERENCES

1. B. Bobbs, M. Matloubian, H.R. Fetterman, R.R. Neurgaonkar and W.K. Cory, *Appl. Phys. Lett.* 48(24), 1642 (1986).
2. W. Ho, W.F. Hall, R.R. Neurgaonkar, R.E. DeWames and T.C. Lim, *Ferroelectrics* 38, 833 (1981).
3. M. Klein in *Infrared and Millimeter Waves*, ed. by K. Button, v. 9, p. 133 (Academic, NY, 1983).
4. R.R. Neurgaonkar and W.K. Cory, *J. Opt. Soc. Am. B* 3, 274 (1986).
5. R.R. Neurgaonkar and W.K. Cory, "Progress in Photorefractive Tungsten Bronze Crystals," *J. Opt. Soc. Am. B* 3(2), 274 (1986).
6. G. Burns and F.H. Dacol, "Glassy Polarization in $K_2Sr_4(NbO_3)_{10}$ -Type Ferroelectrics," *Phys. Rev. B* 30(7), 4012 (1984).
7. A.V. Turik and N.B. Shevchanko, "Dielectric Spectrum of $BaTiO_3$ Single Crystals," *Phys. Stat. Sol. B* 95, 585 (1979).
8. G.D. Boyd, T.J. Bridges, M.A. Pollack and E.H. Turner, "Microwave Nonlinear Susceptibilities Due to Electronic and Ionic Anharmonicities in Acentric Crystals," *Phys. Rev. Lett.* 26 (7), 387 (1971).
9. M.B. Klein, "Phase Shifting at 94 GHz Using the Electro-Optic Effect in Bulk Crystals," *Int. J. IR and MM Waves*, 2(2), 239 (1981).
10. H.M. Chan and M.P. Harmer, IEEE Int'l Symposium on the Applications of Ferroelectrics (ISAF), Lehigh U. (1986).

APPENDIX-1

STRUCTURAL AND FERROELECTRIC PROPERTIES OF MORPHOTROPIC PHASE
BOUNDARY SYSTEMS IN THE TUNGSTEN BRONZE FAMILY

J. R. OLIVER, R. R. NEURGAONKAR AND G. L. SHOOP
PROC. OF IEEE, FERROELECTRICS, 1986(ACCEPTED)

STRUCTURAL AND FERROELECTRIC PROPERTIES OF MORPHOTROPIC PHASE BOUNDARY SYSTEMS
IN THE TUNGSTEN BRONZE FAMILY

J.R. Oliver, R.R. Neurgaonkar and G.L. Shoop

Rockwell International Science Center
Thousand Oaks, CA 91360 U.S.A.

Abstract

Morphotropic phase boundary (MPB) ferroelectric materials are well known to possess enhanced ferroelectric properties, such as their dielectric, piezoelectric and electro-optic characteristics, because of the proximity of an alternate ferroelectric state. In the tungsten bronze structural family, the best known morphotropic system to date has been $Pb_{1-x}Ba_xNb_2O_6$, which has an MPB at $x = 0.37$. Because of the wide variety of solid solutions with differing structural phases available in the bronze family, the potential exists for numerous other morphotropic systems from the binary combination of bronze end-member phases such as $PbNb_2O_6$, $Pb_2KNb_5O_{15}$, $Sr_2NaNb_5O_{15}$, $Ba_2NaNb_5O_{15}$, etc. MPB compositions have been found for many of these binary systems, and structural and ferroelectric data are presented for sintered ceramics based on three of these systems. Potential applications of these morphotropic materials are discussed, along with anticipated bulk single crystal growth problems.

1. Introduction

Several of the more interesting tungsten bronze oxide ferroelectric systems show MPBs, which depend primarily on composition rather than on temperature. Ceramic or single crystal compositions adjacent to such boundaries can show considerable enhancement of electro-optic, dielectric, piezoelectric, electromechanical and pyroelectric properties because of the proximity in energy of an alternate ferroelectric structure. Perhaps the best known MPB bronze system to date is $Pb_{1-x}Ba_xNb_2O_6$ (PBN) which has been grown and evaluated in both single crystal [1,2] and densified ceramic forms [3]. The exceptionally interesting theoretical and experimental aspects of morphotropic PBN have spurred the investigation of other lead-containing pseudo-binary bronze systems based on the following end members:

1. $Ba_2NaNb_5O_{15}$ (BNN)
2. $Sr_2NaNb_5O_{15}$ (SNN)
3. $Pb_2KNb_5O_{15}$ (PKN)
4. $PbNb_2O_6$ (PN)

PKN-BNN

A potentially important tungsten bronze ferroelectric material is PKN. This composition has been grown successfully in hot-pressed dense ceramic form by Nagata et al [4] with a high electromechanical coupling constant, $k_t = 0.40$, and good polarization. As such, it represents an attractive candidate for SAW, piezoelectric and pyroelectric device applications. PKN has also been grown in single crystal form [5], but compositional homogeneity has been a significant problem due to Pb^{2+} volatility at the melt temperature.

Ceramic PKN prepared in this laboratory shows an orthorhombic structure with $a = 17.835\text{\AA}$, $b = 17.944\text{\AA}$ and $c = 3.938\text{\AA}$. The orthorhombic structure of PKN presents the possibility of attaining an MPB condition in combination with another tetragonal or pseudo-tetragonal tungsten bronze composition such as BNN [6]. BNN has been shown to be a good ferroelectric material for electro-optic and nonlinear optic applications, particularly for second harmonic generation of near-IR laser radiation. Stoichiometric BNN is weakly orthorhombic at room temperature with lattice constants $a = 17.592\text{\AA}$, $b = 17.626\text{\AA}$ and $c = 3.995\text{\AA}$ [7]. Above 260°C , an orthorhombic-to-tetragonal transformation occurs at which microtwinning is usually observed in single crystals, but with no significant dielectric anomalies. The Curie point is at $\sim 570^\circ\text{C}$.

An investigation of the pseudo-binary join $(1-x)\text{PKN}-(x)\text{SNN}$ was undertaken using cold-pressed and sintered ceramic materials. Initially, microcracks were observed in nearly all ceramic samples across the compositional range, even with sintering temperatures lowered below 1200°C . However, the addition of excess PbO , on the order of 2-4%, was found to dramatically improve the quality of the ceramics prepared. Measured weight losses showed a 1-2% Pb^{2+} deficiency after sintering for 4 h at $1200-1380^\circ\text{C}$, depending on composition.

Dielectric measurements on ceramic PKN-BNN compositions were made over the range 100 Hz-100 kHz using sputtered Pt electrodes. Dielectric data for the measured Curie point, T_c , and Curie temperature, θ , as a function of composition are shown in Fig. 1. A sharp minimum was observed for T_c at the morphotropic (0.75) PKN-(0.25)BNN compo-

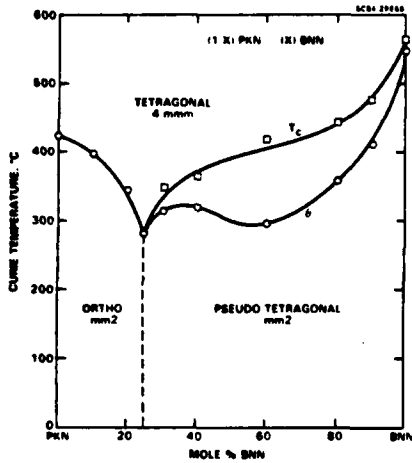


Fig. 1 Phase diagram for the $(1-x)\text{PKN}-(x)\text{BNN}$ system.

sition, where $T_c = 280^\circ\text{C}$. The system shows second-order phase transition behavior ($T_c = \theta$) on the orthorhombic (PKN-rich) side of the MPB, and first-order behavior on the pseudo-tetragonal side. This second to first order change is largely responsible for the steep decline of the dielectric constant at the Curie point, as shown in Fig. 2. The peak in the dielectric constant at room temperature, on the other hand, is due to the rapid decline of T_c and θ on the orthorhombic side of the composition up to the MPB, followed by a change to first order with a rapid increase of θ and a decrease of the Curie-Weiss constant, C_c , as shown in Fig. 3.

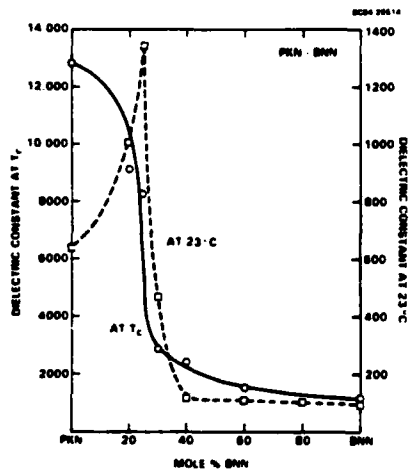


Fig. 2 Dielectric constant at T_c and 23°C for the $(1-x)\text{PKN}-(x)\text{BNN}$ system.

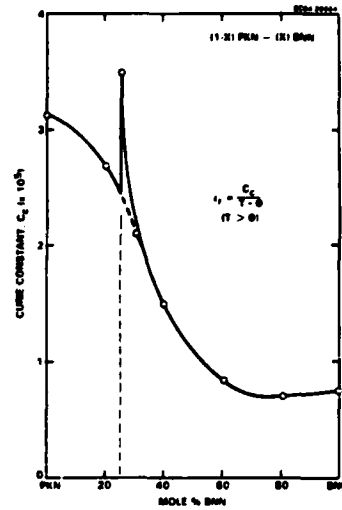


Fig. 3 Curie-Weiss constant for the $(1-x)\text{PKN}-(x)\text{BNN}$ system.

The pronounced dielectric behavior near the MPB is consistent with the abrupt change in the b and c lattice parameters determined from powder x-ray analysis, as shown in Fig. 4. Compositions near the MPB in the PKN-BNN system could be very attractive for both pyroelectric ($x > 0.25$) and electro-optic ($x < 0.25$) applications. Certainly, single crystal growth of this material would be desirable, although as a high Pb-content solid solution, Czochralski growth may be difficult.

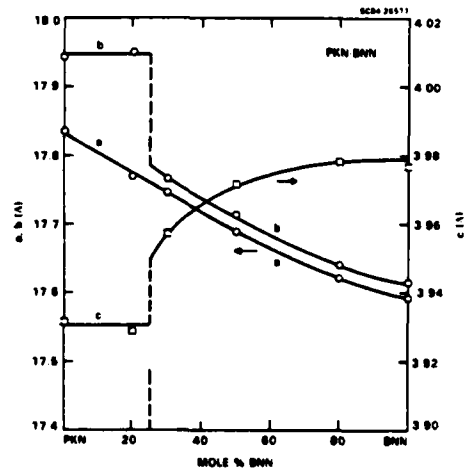


Fig. 4 Lattice parameters for PKN-BNN.

PKN-SNN

An alternative pseudo-binary end member for PKN is SNN [6]. X-ray analysis of SNN ceramic powders show a weak but consistent orthorhombic lattice distortion with $a = 17.448\text{Å}$, $b = 17.487\text{Å}$ and $c = 3.895\text{Å}$. Ceramic samples for the join

(1-x)PKN-(x)SNN were sintered at 1200-1260°C with no significant cracking. Dielectric measurements of T_c and θ as a function of composition are shown in Fig. 5, where a broad minimum in T_c (155°C) is observed for $0.70 < x < 0.75$. Second-order phase transition behavior was found up to $x = 0.75$, beyond which the transition becomes first order ($T_c > \theta$). This change from second to first order

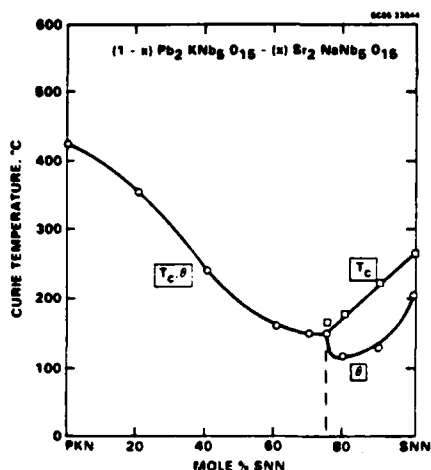


Fig. 5 Phase diagram for the (1-x)PKN-(x)SNN system.

is reflected in the dielectric behavior at T_c and at room temperature, shown in Fig. 6, where ϵ decreases rapidly for $x > 0.75$. For compositions near $x = 1$ (pure SNN), there is a dramatic increase in the room temperature dielectric value resulting from a broad, low temperature transition (below 0°C); evaluation of modified SNN bulk crys-

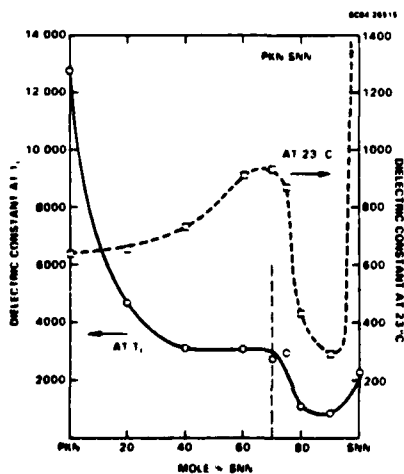


Fig. 6 Dielectric constant at T_c and 23°C for the (1-x)PKN-(x)SNN system.

tals grown in our laboratory [8] suggests that this is a ferroelastic phase transition.

Figure 7 shows the Curie-Weiss constant as a function of composition, where a sharp discontinuity is seen at $x = 0.75$. However, lattice parameter analysis of x-ray powder diffraction data, shown in Fig. 8, shows only a gradual change in the a and b lattice parameters near $x = 0.75$, where they become indistinguishable. Since this change appears to be so gradual, it is presently questioned whether the (0.25)PKN-(0.75)SNN composition is truly morphotropic. Nevertheless, the phase transition temperature and Curie-Weiss

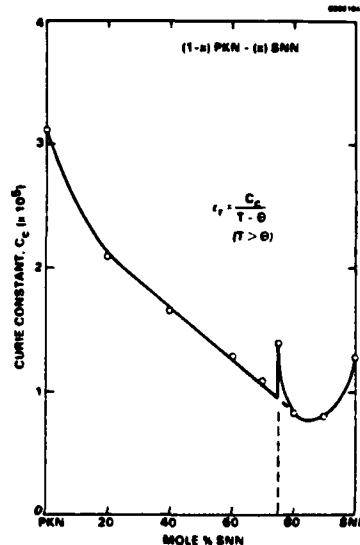


Fig. 7 Curie-Weiss constant for the (1-x)PKN-(x)SNN system.

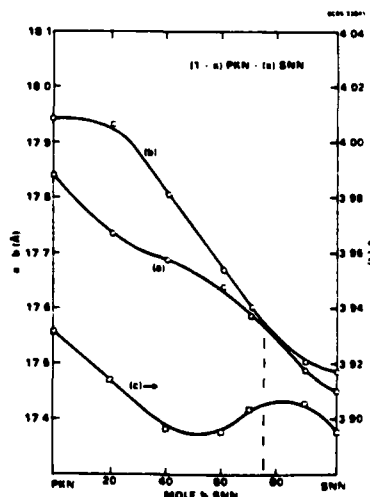


Fig. 8 Lattice parameters for PKN-SNN.

behavior as a function of composition strongly suggest a classic morphotropic phase boundary at $x = 0.70-0.75$. The high room temperature dielectric values near this region make the PKN-SNN system very attractive for electro-optic and millimeter-wave applications.

PN-SNN

PN is a widely studied orthorhombic bronze which has already been found to have a morphotropic phase boundary in the $(1-x)PN-(x)BN$ system at $x = 0.37$ [1,2]. An apparent MPB has now also been found for a new system, $(1-x)PN-(x)SNN$ at $x = 0.70-0.75$, as shown in Fig. 9. The decrease in the phase transition temperature T_c at the MPB is quite dramatic, going from 565°C for pure PN down to 135°C at $x = 0.75$. The Curie-Weiss behavior is first order over the entire compositional range, with large differences between T_c and θ only near the end members. As a result, dielectric maxima are large, on the order of 8000-12000, over most of the compositional range.

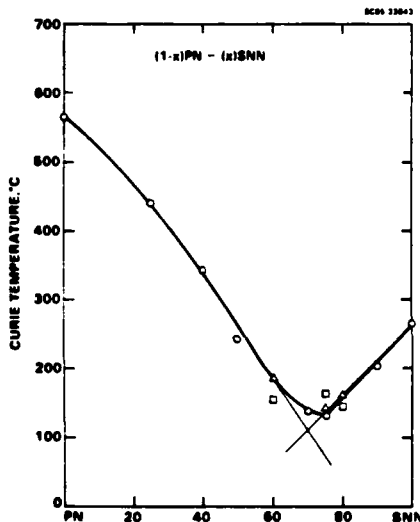


Fig. 9 Phase diagram for the $(1-x)PN-(x)SNN$ system.

The room temperature dielectric constant, shown in Fig. 10, peaks sharply at $x = 0.75$ with $\epsilon = 3400$. This maximum is due to the minimum T_c value and to a peak in the Curie-Weiss constant at $x = 0.70$, as shown in Fig. 11, which gives rise to a broadening of the dielectric phase transition anomaly near the MPB.

2. Discussion

Both the PKN-SNN and PN-SNN systems look to be very promising candidates for single crystal development. A major advantage in both systems is that the more interesting compositions occur on the SNN-rich side of the phase diagram, making homogeneous crystal growth a significantly easier task. Nevertheless, Pb^{2+} volatility at the melt temperature is still a major concern, and more

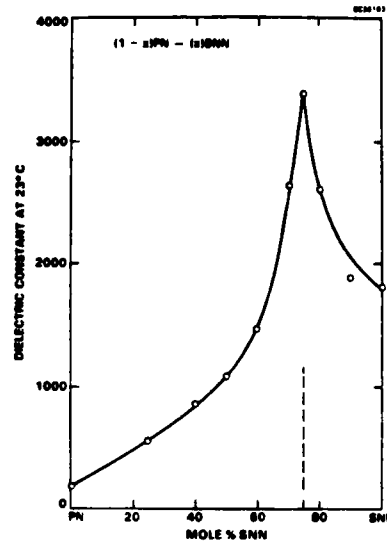


Fig. 10 Dielectric constant at 23°C for the $(1-x)PN-(x)SNN$ system.

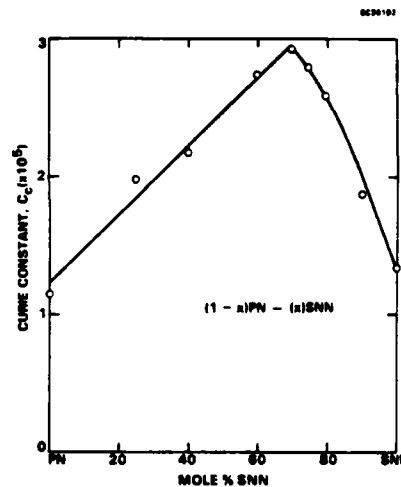


Fig. 11 Curie-Weiss constant for the $(1-x)PN-(x)SNN$ system.

work is necessary to accurately evaluate Pb^{2+} losses prior to Czochralski crystal growth. All of the tungsten bronze systems examined possess high dielectric constants at room temperature, implying a high potential value in future optical and millimeter-wave applications.

3. Acknowledgements

This work was supported in part by the Office of Naval Research, Contract No. N00014-81-C-0463, DARPA, Contract No. N00014-82-C-2466, and Rockwell Internal Research & Development. The authors would like to thank Dr. L.E. Cross for his valuable discussions on this research.

4. References

- [1] T.R. Shrout, H. Chen and L.E. Cross, "Dielectric and Piezoelectric Properties of $Pb_{1-x}Ba_xNb_2O_6$ Ferroelectric Tungsten Bronze Crystals," *Ferroelectrics* 56, 45-48, (1983).
- [2] T.R. Shrout and L.E. Cross, "Ferroelectric Properties of Tungsten Bronze Lead Barium Niobate (PBN) Single Crystals," *Ferroelectrics Lett.* 44, 325-330, (1983).
- [3] M. Yokosuka, "A New Transparent Ferroelectric Ceramic, Lanthanum-Modified Lead Barium Metaniobate (PBLN)," *Japan. J. Appl. Phys.* 16 (2), 379-380, (1977).
- [4] K. Nagata, T. Yamazaki and K. Okazaki, "Dielectric and Piezoelectric Properties of Hot-Pressed Lead Potassium Niobate," in Proc. 2nd Meeting on Ferroelectric Materials and Their Applications, No. F-10, 251-256, (1979).
- [5] J. Nakano and T. Yamada, "Ferroelectric and Optical Properties of Lead Potassium Niobate," *J. Appl. Phys.* 46 (6), 2361-2365, (1975).
- [6] J.E. Geusic, A.J. Levenstein, J.J. Rubin, S. Singh and L.G. Van Uitert, "The Non-linear Optical Properties of $Ba_2NaNb_5D_{15}$," *Appl. Phys. Lett.* 11 (9), 269-271, (1967).
- [7] R.L. Barnes, "Barium Sodium Niobate ($Ba_{(4+x)}Na_{(2-2x)}Nb_{10}O_{30}$) Crystallographic Data and Thermal Expansion Coefficients," *J. Appl. Cryst.* 1, 290-292, (1968).
- [8] R.R. Neurgaonkar, J.R. Oliver, W.K. Cory and L.E. Cross, unpublished data.

APPENDIX- 2

MILLIMETER WAVE DIELECTRIC PROPERTIES OF TUNGSTEN BRONZE FERRO-
ELECTRICS AT 77K and 300 K

W. F. HALL, W. W. HO, R. R. NEURGAONKAR AND W.K. CORY
PROC. OF IEEE, FERROELECTRICS, 1986 (ACCEPTED)

MILLIMETER WAVE DIELECTRIC PROPERTIES OF TUNGSTEN BRONZE FERROELECTRICS AT 77 AND 300 K*

W.F. Hall, W.W. Ho, R.R. Neurgaonkar, and W.K. Cory

Rockwell International Science Center
Thousand Oaks, California 91360 U.S.A.

Abstract

Results of measurements of dielectric permittivity, dielectric loss, and electric field sensitivity of the polar axis refractive index of tungsten bronze ferroelectrics are presented for frequencies from 30 to 135 GHz and for temperatures of 77 and 300 K. A model for the microwave loss is compared with observations.

1. Dielectric Permittivity and Loss

Ferroelectric materials exhibit a variety of unusual effects connected with their structural phase transitions. The interrelations among these effects have been well accounted for in the phenomenological free energy models of Landau, Ginsberg, and Devonshire. Combining such a model with the soft-mode description of the ferroelectric phase transition leads to a prediction for the frequency dependence of ferroelectric properties such as dielectric permittivity, loss tangent, and electric field sensitivity. It has been a primary thrust of our investigations over the past five years to test these predictions for a particular class of ferroelectrics, the tungsten bronzes, at millimeter wave frequencies.

In our laboratory, considerable effort has been devoted to developing growth techniques for tungsten bronze ferroelectrics, and single crystals of large size are now available for several different compositions. Figure 1 shows on a phase diagram some of the major ferroelectrics which we have selected for further study. Our millimeter wave dielectric measurements are being carried out primarily on the various compositions of barium strontium potassium sodium niobate (BSKNN) and strontium barium niobate (SBN). A detailed description of the growth and characterization of these materials is given elsewhere [1].

The dielectric permittivity (ϵ') and loss (ϵ'') for two compositions of BSKNN and SBN are summarized in Table I for room temperature (295 K) and liquid nitrogen temperature (77 K). Measurements were made at various frequencies above 30 GHz as noted in the table. In obtaining these results, waveguide transmission and reflection on samples filling the guide were used below 50 GHz,

* This work is supported by the Office of Naval Research under Contract No. N00014-81-C-0463

while free space measurements of reflected and transmitted power were used above 90 GHz.

The features common to all the ferroelectrics we have studied include:

- 1) A large decrease in polar axis permittivity from its dc value
- 2) A large polar axis dielectric loss
- 3) A large temperature dependence of these properties
- 4) Perpendicular to the polar axis, the loss is smaller at room temperature but remains high on cooling, while the permittivity stays much closer to its dc value.

This behavior is generally not predicted by the soft-mode model, and suggests that a millimeter wave relaxation mechanism is responsible for a majority of the observed dc polarizability along the polar axis.

We have considered in some detail a model based on the notion that there is substantial variation in the direction and magnitude of the spontaneous polarization within a poled single crystal, probably as a result of the microscopic variations in composition which arise naturally in solid solution systems. Experimental evidence for such departures from uniform polarization can be found in the recent publications of Burns and Dacol [2].

To obtain a qualitative understanding of the predictions of this model, we have calculated the polar axis microwave loss for an array of microdomains of reversed polarization scattered throughout the crystal. Essentially, the microwave electric field does mechanical work on the charge trapped at the domain walls, which shows up in the form of damped acoustic waves in the crystal. A similar model for polydomain loss has been proposed by Turik and Shevchenko [3]. We do not assume any field-induced reversal of the local polarization.

The resulting form of the microwave loss can be represented schematically as

$$\epsilon'' = [2Q(\epsilon' - \epsilon_0)P_0]^2 \epsilon^P \left(\frac{d_0}{s}\right) (f(\omega d/v, \omega\eta))_d,$$

where Q is the appropriate electrostriction constant for a particular orientation of the applied field, ϵ^P is the appro-

priate elastic modulus, P_0 is the spontaneous polarization, d_0 is the average domain size along the polar axis, s is the inverse of the number of domain walls per unit length, v is the sound velocity for longitudinal acoustic waves, and η is the elastic damping for these waves. The resonance function f has a complicated structure which on averaging over domain size reduces to the Debye relaxor form at low and high frequency, with a relaxation time given by $\tau = d_0/v$.

A significant qualitative feature of this loss model is the scaling of the loss ϵ'' with the square of the high-frequency permittivity. Table II shows the behavior of this ratio for three tungsten bronze crystals at 30–50 GHz. One should note particularly that the two BSKNN compositions have identical ratios at a given temperature, although the absolute values of ϵ'' differ by a factor of two. The trend in these ratios with temperature is also interesting, and suggests that the number of reversed domains is increasing as $(T_c - T)^2$ as the Curie temperature is approached.

The actual magnitude of the millimeter wave loss, as derived from this expression for the tungsten bronzes, is too small by about a factor of three to account for the observed dispersion. However, the trends are very suggestive, and it is reasonable to expect that extending the model to include polarization reversal will yield better quantitative agreement.

2. Electric Field Sensitivity

Polarized ferroelectrics exhibit a linear dependence of their dielectric permittivity ϵ' or refractive index n on applied dc electric field strength, arising from the additional polar axis polarization induced by the field. Very few measurements of this effect have been made at millimeter wave frequencies since the early work of Boyd, et al. [4]. Klein [5] has examined lithium niobate and, more recently, barium titanate. We have made measurements over a range of

frequencies on $\text{Sr}_{0.61}\text{Ba}_{0.39}\text{Nb}_2\text{O}_6$ (SBN:60) as samples of sufficient size became available from our materials development research, and most recently we have measured $\text{Ba}_{0.8}\text{Sr}_{1.8}\text{K}_{0.8}\text{Na}_{0.8}\text{Nb}_5\text{O}_{18}$ (BSKNN-II) between 125 and 135 GHz.

A summary of the polar axis sensitivity, dn_3/dE_3 , for these two materials is given in Table III. The room temperature values are roughly consistent with the dc phenomenological model of the tungsten bronzes proposed by L.E. Cross. The generalization of Miller's rule proposed by Boyd [4], which states that dn/dE should be proportional to n^6 , appears to work well in comparing the room temperature and 77 K values of dn/dE for BSKNN-II, but not well at all for SBN:60. It will be interesting to see how other tungsten bronzes fit this scheme. For most device applications of this effect, one seeks both large sensitivity and low loss, and reliable guidelines for the selection of appropriate materials for growth would greatly benefit this work.

References

- [1] R.R. Neurgaonkar and W.K. Cory, "Progress in photorefractive tungsten bronze crystals," J. Opt. Soc. Am. B 3 (2), 1986, pp. 274–282.
- [2] G. Burns and F.H. Dacol, "Glassy polarization in $\text{K}_2\text{Sr}_4(\text{NbO}_3)_{10}$ -type ferroelectrics," Phys. Rev. B 30 (7), 1984, pp. 4012–4013.
- [3] A.V. Turik and N.B. Shevchenko, "Dielectric spectrum of BaTiO_3 single crystals," Phys. Stat. Sol. B 95, 1979, pp. 585–592.
- [4] G.D. Boyd, T.J. Bridges, M.A. Pollack, and E.H. Turner, "Microwave nonlinear susceptibilities due to electronic and ionic anharmonicities in acentric crystals," Phys. Rev. Lett. 26 (7), 1971, pp. 387–390.
- [5] M.B. Klein, "Phase shifting at 94 GHz using the electro-optic effect in bulk crystals," Int. J. IR and MM Waves, 2 (2), 1981, pp. 239–246.

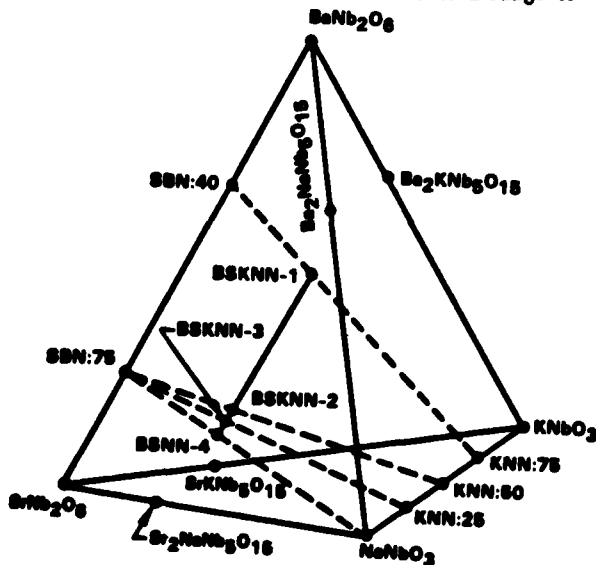


Figure 1.
Phase Diagram Illustrating Tungsten
Bronze Compositions Selected for Study

Table I. Millimeter Wave Dielectric Properties of Single Crystal BSKNN and SBN

Axis	Temp. ($^{\circ}$ K)	BSKNN-II*		SBN:60**		Frequency	
		ϵ'	ϵ''	ϵ'	ϵ''		
c	295	95	18	158	86	30-50 GHz	
	77	39	2	124	8.8		
a	295	427	81	231	51		
	77	418	70	190	37		
c	295	93	26	273	149		BSKNN: 125-135 GHz
	77	36	2.5	67	23		
a	295	430	80	211	37	SBN: 90-100 GHz	
	77			180	29		

* $Ba_{0.5}Sr_{1.5}K_{0.5}Na_{0.5}Nb_3O_{15}$

** The low and high frequency samples of SBN:60 are from two different growths. Large boule-to-boule variations in permittivity have been found.

Table II. Trends in Polar Axis Permittivity Compared with Acoustic Loss Model

	BSKNN-I	BSKNN-II	SBN: 60
Room T	2.2×10^{-2}	2.0×10^{-2}	3.4×10^{-2}
Liquid N ₂	1.2×10^{-2}	1.3×10^{-2}	0.6×10^{-2}
Variation with Temperature			
RT/LN ₂	1.8	1.5	5.7
$(T_c - LN_2)/(T_c - RT)$	2.2	2.5	5.1

Table III. Electric Field Sensitivity of the Polar Axis Refractive Index at 100 GHz

	BSKNN-II		SBN:60	
	dn/dE	n	dn/dE	n
Room T	4×10^{-7} m/V	9.8	1.6×10^{-8} m/V	17.1
Liquid N ₂	4.3×10^{-8} m/V	6.25	5.0×10^{-7} m/V	8.3
Comparison with Boyd's Rule				
$dn/dE(RT/LN_2)$	9.3		3.2	
$(n_{RT}/n_{LN_2})^5$	9.5		37	

END

12-86

DTIC